NAVAL POSTGRADUATE SCHOOL

MONTEREY, CALIFORNIA

THESIS

IMPROVING DIGITAL HIGH FREQUENCY (HF) COMMUNICATIONS WITH MULTI-DIMENSIONAL CONSTANT ENERGY MODULATION IMPLEMENTATION

by

Adam J. Waymouth

September 2020

Thesis Advisor: Ric Romero
Co-Advisor: Tri T. Ha

THIS PAGE INTENTIONALLY LEFT BLANK

REPORT DOCUMENTATION PAGE			*Form Approved OMB No. 0704-0188*

1. AGENCY USE ONLY ***(Leave blank)***	**2. REPORT DATE** September 2020	**3. REPORT TYPE AND DATES COVERED** Master's thesis

4. TITLE AND SUBTITLE
IMPROVING DIGITAL HIGH FREQUENCY (HF) COMMUNICATIONS WITH MULTI-DIMENSIONAL CONSTANT ENERGY MODULATION IMPLEMENTATION

5. FUNDING NUMBERS
RENUT

6. AUTHOR(S) Adam J. Waymouth

7. PERFORMING ORGANIZATION NAME(S) AND ADDRESS(ES)
Naval Postgraduate School
Monterey, CA 93943-5000

8. PERFORMING ORGANIZATION REPORT NUMBER

9. SPONSORING / MONITORING AGENCY NAME(S) AND ADDRESS(ES)
Navy Information Warfare Command, San Diego, CA 92152

10. SPONSORING / MONITORING AGENCY REPORT NUMBER

11. SUPPLEMENTARY NOTES The views expressed in this thesis are those of the author and do not reflect the official policy or position of the Department of Defense or the U.S. Government.

12a. DISTRIBUTION / AVAILABILITY STATEMENT
Approved for public release. Distribution is unlimited.

12b. DISTRIBUTION CODE
A

13. ABSTRACT (maximum 200 words)

Improved high frequency (HF) digital communication is desired in commercial and military applications, especially at sea where the primary digital communications is satellite communications (SATCOM). HF over-the-horizon (OTH) relays are often the alternative communication path when SATCOM is too costly or not available. Our work suggests using multiple-input multiple-output (MIMO), orthogonal frequency division multiplexing (OFDM), and various modulations in HF OTH communications to reduce the bit error rate (BER), improve data throughput in the allocated bandwidth, and potentially provide physical layer security through obfuscation. We implement MIMO, OFDM, and multi-dimensional constant energy modulation (CEM) by utilizing GNU Radio Companion (GRC) to program two NI Ettus X310 Software Defined Radios (SDR) in a 2x2 MIMO configuration. This is the first time CEM has been transmitted and received. Modulation and demodulation are successful for various file types. The 4D-16 CEM constellation and its BER are compared to that of quadrature phase shift keying (QPSK) and 16-quadrature amplitude modulation (QAM). Explanations of how CEM, OFDM subcarriers, and space time block codes (STBC) can provide frequency agility, throughput manipulation, and physical layer security are provided. Selected CEM constellations are presented.

14. SUBJECT TERMS
multiple-input multiple-output, MIMO, orthogonal frequency division multiplexing, OFDM, modulation, high frequency, HF, multi-dimensional, digital communication, GNU, GNU Radio Companion, GRC, Software Defined Radio, SDR, X310, fading, FPGA, field programmable gate array, QPSK, quadrature phase shift keying, QAM, quadrature amplitude modulation, STBC, space time block code, BER, bit error rate, SATCOM, satellite communication, OTH, over-the-horizon

15. NUMBER OF PAGES
75

16. PRICE CODE

17. SECURITY CLASSIFICATION OF REPORT	**18. SECURITY CLASSIFICATION OF THIS PAGE**	**19. SECURITY CLASSIFICATION OF ABSTRACT**	**20. LIMITATION OF ABSTRACT**
Unclassified	Unclassified	Unclassified	UU

NSN 7540-01-280-5500

Standard Form 298 (Rev. 2-89)
Prescribed by ANSI Std. 239-18

THIS PAGE INTENTIONALLY LEFT BLANK

Approved for public release. Distribution is unlimited.

IMPROVING DIGITAL HIGH FREQUENCY (HF) COMMUNICATIONS WITH MULTI-DIMENSIONAL CONSTANT ENERGY MODULATION IMPLEMENTATION

Adam J. Waymouth
Lieutenant Commander, United States Navy
BS, U.S. Naval Academy, 2011

Submitted in partial fulfillment of the
requirements for the degree of

MASTER OF SCIENCE IN ELECTRICAL ENGINEERING

from the

NAVAL POSTGRADUATE SCHOOL
September 2020

Approved by: Ric Romero
Advisor

Tri T. Ha
Co-Advisor

Douglas J. Fouts
Chair, Department of Electrical and Computer Engineering

THIS PAGE INTENTIONALLY LEFT BLANK

ABSTRACT

Improved high frequency (HF) digital communication is desired in commercial and military applications, especially at sea where the primary digital communications is satellite communications (SATCOM). HF over-the-horizon (OTH) relays are often the alternative communication path when SATCOM is too costly or not available. Our work suggests using multiple-input multiple-output (MIMO), orthogonal frequency division multiplexing (OFDM), and various modulations in HF OTH communications to reduce the bit error rate (BER), improve data throughput in the allocated bandwidth, and potentially provide physical layer security through obfuscation. We implement MIMO, OFDM, and multi-dimensional constant energy modulation (CEM) by utilizing GNU Radio Companion (GRC) to program two NI Ettus X310 Software Defined Radios (SDR) in a 2x2 MIMO configuration. This is the first time CEM has been transmitted and received. Modulation and demodulation are successful for various file types. The 4D-16 CEM constellation and its BER are compared to that of quadrature phase shift keying (QPSK) and 16-quadrature amplitude modulation (QAM). Explanations of how CEM, OFDM subcarriers, and space time block codes (STBC) can provide frequency agility, throughput manipulation, and physical layer security are provided. Selected CEM constellations are presented.

THIS PAGE INTENTIONALLY LEFT BLANK

Table of Contents

List of Figures

List of Tables

THIS PAGE INTENTIONALLY LEFT BLANK

List of Acronyms and Abbreviations

BER	bit error rate
CEM	multi-dimensional constant energy modulation
DSP	digital signal processing
FEC	forward error correction
FFT	fast Fourier transform
FPGA	field-programmable gate array
GPSDO	Global Positioning System disciplined oscillator
GRC	GNU Radio Companion
HDL	hardware description language
HF	high frequency
ISI	inter-symbol interference
IFFT	inverse fast Fourier transform (FFT)
LOS	line of sight
MHPSK	M-ary hyper phase shift keying
MF	medium frequency
MIMO	multiple-input multiple-output
NIC	network interface card
OFDM	orthogonal frequency division multiplexing
OTH	over-the-horizon
QAM	quadrature amplitude modulation
QPSK	quadrature phase shift keying
RF	radio frequency
RX	receive
SATCOM	satellite communication

SDR	software defined radio
SNR	signal-to-noise ratio
STBC	space time block code
TX	transmit
USRP	universal software radio peripheral
VSG	vector signal generator

Acknowledgments

Thank you, Prof Ric Romero, Prof Tri Ha, LCDR Mike Cribbs, and LT Vikram Kanth, for your critical support; this research would not be completed without your comprehensive lessons and extensive technical help.

Thank you, Prof Douglas Fouts, Prof Jim Scofani, and LCDR Ted Haskell, for synergizing our research efforts; I believe the Department of Defense will benefit more from our research because of it.

Thank you, Bruce Chiarelli and Michael Dickens, for your exceptional skills supporting the hardware setup and configuration of the X310 software defined radios.

Thank you, CDR Clay Herring, Prof Monique Fargues, and Julie Samples, for quality academic guidance. There isn't a better academic team.

Finally, thank you to all of the people and organizations at NPS who have enriched my time outside of academics and helped make lasting memories in Monterey: PBSA, NPSAAF Outdoors and Maker's Clubs, Scott Bischoff, Diane Jones, Carmen, Canisio, Ashton, Eric, Tony, Brian, Beth, Travis, Marje, Ida, Chris, and Logan. Fair winds and following seas (until we meet again).

THIS PAGE INTENTIONALLY LEFT BLANK

CHAPTER 1:
Introduction

The use of the frequency spectrum is managed in the United States by the FCC [1] and competing demands from corporate, government, military, and amateur radio operators constrain frequency allocation. Optimizing the allocated spectrum has the potential to increase the number of signals, data throughput, and spectral efficiency in designated bandwidths. This can improve support for end-to-end systems and associated applications, especially for over-the-horizon (OTH) scenarios.

Commercial and military ships at sea must maintain communications over large distances. Long range communications links may be established through costly satellite relays or through less capable OTH medium frequency (MF) and high frequency (HF) links [2]. The ionospheric conditions commonly force satellite communication (SATCOM) to higher frequency bands, which also benefit from higher data rates. The physical characteristics of the Earth and related propagation effects enable the use of frequency bands under the maximum usable frequency for OTH communications, but these bands naturally have lower data rates. In addition, OTH communications are prone to suffer low signal-to-noise ratio (SNR) from fading channels and other distortion effects, which do not affect SATCOM as severely [1].

Increasing the spectral efficiency in HF digital communications can help close the capability gaps between traditional OTH and SATCOM, thus providing a more reasonable alternative than current HF communications when SATCOM is not feasible or is degraded. Motivation for increased throughput, reliability, and capability of HF links, especially during SATCOM denied environments, is elaborated in [2], [3].

1.1 Objectives

To address these concerns, this research uses GNU Radio Companion (GRC) flowgraphs to program two NI Ettus X310 software defined radios (SDRs) with multi-dimensional constant energy modulation (CEM), orthogonal frequency division multiplexing (OFDM), and multiple-input multiple-output (MIMO) capabilities in a 2x2 MIMO configuration. HF fre-

quencies are utilized for transmission. Additionally, this work implements the foundational radio frequency (RF) circuit used for ongoing research in space time block code (STBC) physical layer security [4], which can benefit from using CEM to improve the spectral efficiency and bit error rate (BER) in non-linear channels [5], [6]. Additionally, CEM can be used with OFDM frequency agility to maintain acceptable data throughput [7].

In this work, CEM, as a viable modulation, is successfully implemented for the first time in a live communications circuit. Moreover, multiple file types are successfully tested.

1.2 Scope and Organization

Chapter 2 contains channel and transmission considerations. It introduces digital HF communications with emphasis on fading channels. MIMO is proposed as a diversity scheme to address fading channels. Hardware selection for MIMO considerations is included. OFDM is discussed to introduce subcarriers and how subcarriers are used in CEM transmission.

Chapter 3 contains hardware and software setups used in this research. Emphasis is on SDR hardware components and utilized configurations. GRC is introduced.

Chapter 4 contains CEM theory and describes implementation. The intent and conclusions of prior CEM research are provided in addition to an explanation of CEM constellations based on Euclidean distance and Gray coded symbol mapping. Baseband CEM modulation and demodulation flowgraphs are presented. The 4D-16 CEM constellation and its BER are compared to that of quadrature phase shift keying (QPSK) and 16-quadrature amplitude modulation (QAM). Constellations of select baseband and transmitted CEM symbols are presented and analyzed.

Chapter 5 continues the stages of implementation with MIMO-OFDM CEM flowgraph and results. Additional considerations are included to discuss how a CEM MIMO-OFDM framework can further improve HF communications.

Chapter 6 contains conclusions and recommendations for future works.

CHAPTER 2:
Transmission Considerations

Transmission considerations inform decisions on the hardware and software used in this research. This chapter includes the importance of using HF, MIMO, and OFDM, while introducing background for the hardware and software setups that will be presented in Chapter 3.

2.1 High Frequency

As a modulation scheme, CEM is independent of transmission frequency. However, HF, specifically 20 MHz, is chosen as the center frequency for scenario applicability.

2.1.1 Propagation Effects

HF communications is plagued with interference from propagation, characterized by high attenuation from spherical spreading and by fading from interactions with the ionosphere and environment. Both effects lower the signal power at the receiver. In most cases, attenuation loss can be partially mitigated by increasing power at the transmitter, use of a very low noise amplifier, higher gain antennas for the transmitter and/or receiver, and various signal processing techniques at the receiver. Fading is arguably harder to correct and causes data synchronization issues [1].

2.1.2 Channel Fading

The propagation path for a vessel underway can be affected by the ionosphere or by geographic features, including buildings if the receiver is in an urban environment. Fading in the HF band can vary significantly in location and latitude [8]. All main fading effects should be considered for HF propagation. This research briefly discusses effects of slow, fast, flat, frequency-selective, and deep fading when designing the communications architecture.

Fading occurs in pairs of time-varying and space-varying effects. Time-varying (Doppler) effects define slow versus fast characteristics and space-varying (multipath) effects define flat versus frequency-selective characteristics. [9].

Slow Versus Fast Fading

Doppler effect is due to frequency Doppler shift,

$$f = -f_c v/c, \tag{2.1}$$

where f_c is the carrier frequency, v is the radial velocity, and c is the speed of light in free space. The maximum difference between all positive Doppler shifts, f_i, and all negative Doppler shifts, f_j is the Doppler spread,

$$f_D = \max_{i,j} \left| f_i - f_j \right|. \tag{2.2}$$

The coherence time, which is empirically approximated by

$$T_c = \frac{1}{4 f_D}, \tag{2.3}$$

is related to the Doppler spread and is compared to the measured channel estimation time to determine slow and fast fading. A channel experiences slow fading when the coherence time is greater than the channel estimation time and fast fading when coherence time is less than the channel estimation time.

Flat Versus Frequency-Selective Fading

The multipath effect is characterized by the multipath delay spread,

$$T_d = \max_{MIP} \left[\tau_l(t) - \tau_1(t) | \min_l \{ P_1 / P_l > \gamma \} \right], \tag{2.4}$$

where the multipath intensity profile (MIP) shows power versus delay, P_1 is the power of the first path, $\tau_1(t)$ is the time of the first path, P_l is the power of the last significant path, $\tau_l(t)$ is the time of the last significant path, and γ is the power threshold. The inverse of the multipath delay spread is the coherence bandwidth,

$$B_c = \frac{1}{T_d}. \tag{2.5}$$

Coherence bandwidth is compared to the measured signal bandwidth. Multipath delay spread is compared to the measured symbol time. Either comparison determines flat or

frequency-selective fading. A channel experiences flat fading when the signal bandwidth is less than the coherence bandwidth or the multipath delay spread is less than the symbol time. A channel experiences frequency-selective fading when the signal bandwidth is greater than the coherence bandwidth or the multipath delay spread is greater than the symbol time [9].

Fading Solutions

A notional transmitted and received signal though a fading channel is shown in Figure 2.1; the various fading types and their associated mitigation techniques are presented below the diagram. Flat and frequency-selective fading are mitigated with channel equalization; fast and slow fading are mitigated with diversity schemes; deep fading is mitigated with channel coding. This work uses MIMO to implement channel equalization and diversity schemes [10].

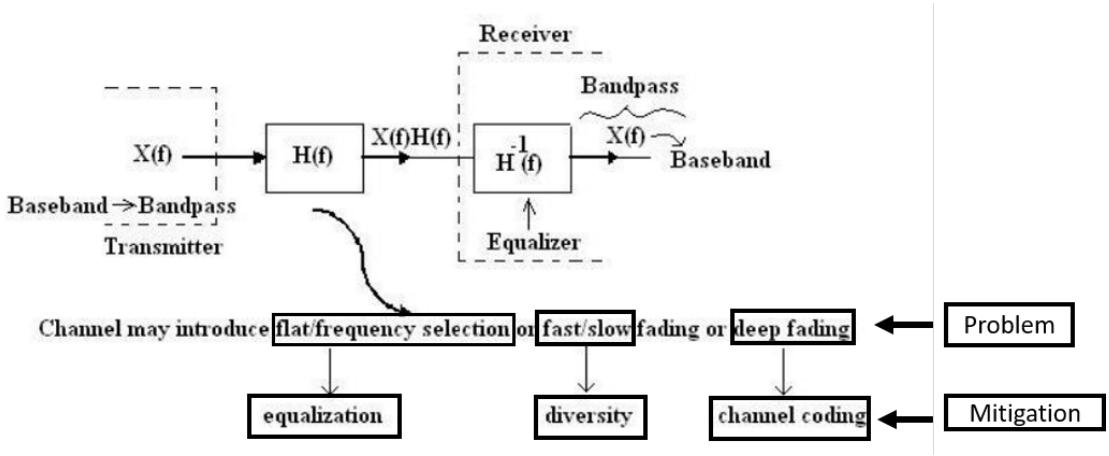

Figure 2.1. Fading types and associated solutions. Adapted from [10].

2.2 Multiple-Input Multiple-Output

MIMO using Alamouti STBCs is chosen to counter the fading effects common in HF propagation.

2.2.1 Channel Estimation

Slow fading is solved with channel estimation. Channel soundings compare the received signal impulse to a transmitted known reference known as a training sequence (OFDM uses

a similar process with sync words as a reference). The difference between the impulse and the reference quantifies the effect of the channel on the signal and is called the channel estimation. A diversity combiner uses channel estimations to cancel channel effects from the noisy signal in order to extract the original signal [1]. This work uses a channel estimator with a MIMO diversity combiner to address fading. A diversity combiner is referred to as a channel equalizer in this work.

2.2.2 Spatial Diversity

Spatial diversity is sending multiple variants of the same signal over multiple propagation paths that have independent fading behaviors. The intent is to mitigate the effects of deep fading since it is unlikely any two propagation paths experience the same exact simultaneous deep fade. Spatial diversity helps guarantee independent propagation paths by physically separating multiple transmit or receive antennas, or by sending the same signal with varying transmission characteristics (differing times, frequencies, or polarizations). MIMO can potentially address all three forms of spatial diversity: physical separation between antennas creates phase offsets, and thus time differences between multiple paths; transmission of different carrier frequencies for each antenna creates frequency diversity; and different orientations for each antenna creates polarization diversity [1].

2.2.3 Alamouti Space Time Block Codes

Space-time block coding techniques like Alamouti code are employed with MIMO to address time and spatial diversity. Alamouti code uses STBCs to make orthogonal copies of each transmission row vector, then transmits the orthogonal copies during the following transmission period, thus accomplishing time difference desired for spatial diversity [1], [9]. Equation (2.6) shows the 2x2 STBC matrix, **G**, composed of orthogonal columns of symbols s_1 and s_2 [9].

$$\begin{array}{c} Antenna1 \ Antenna2 \\ \uparrow \quad \uparrow \\ \mathbf{G} = \begin{bmatrix} s_1 & s_2 \\ -s_2^* & s_1^* \end{bmatrix} \begin{array}{l} \rightarrow Symbol\ time\ 1 \\ \rightarrow Symbol\ time\ 2 \end{array} \end{array} \tag{2.6}$$

2.3 Orthogonal Frequency Division Multiplexing

OFDM is used to occupy the allocated bandwidth, counter fading with a cyclic prefixer, and mitigate narrowband noise in degraded channels. The concept of subcarriers is adapted in this work to transmit CEM symbols.

2.3.1 Subcarriers

Frequency division multiplexing has multiple signal carriers, called subcarriers, that are centered about the signal center frequency. In practice, each subcarrier will be assigned a symbol per unit transmission time. In OFDM, the subcarriers are orthogonally spaced. Adjacent OFDM subcarriers do not interfere with each other (i.e., subcarrier nulls happen to fall on other subcarrier peaks). This is depicted in the analog (right) part of Figure 2.2. Dependent on modulation, OFDM potentially has better data throughput due to two OFDM subcarriers fitting in the same bandwidth compared to that of 1.5 non-OFDM subcarriers [6].

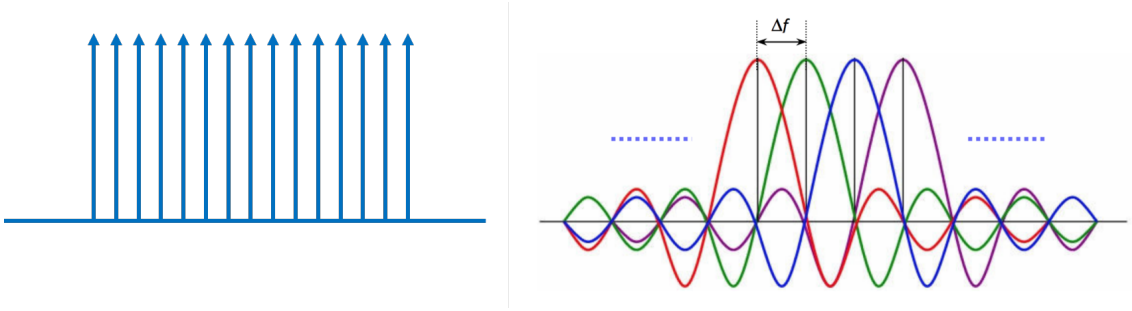

Figure 2.2. OFDM subcarriers in frequency domain; subcarriers shown in digital representation (left) and subcarriers shown in analog representation (right). Source: [7].

2.3.2 Solutions with Orthogonal Frequency Division Multiplexing

The subcarriers in OFDM are important to this work for two reasons: translating multiple dimensions to another domain (or multiple domains), and to avoid severely degraded bands within an allocated spectrum.

The first reason is because CEM is a multi-dimensional modulation, but the complex plane is limited to two dimensions. Therefore, dimension components are paired into complex

values and assigned to subcarriers for transmission in the time domain [5], [6]. More details are explained in Chapter 4.

The second reason is the ability to select which subcarriers contain symbols, and thus improve SNR by omitting subcarriers in a degraded channel [7]. More details are explained in Chapter5.

CHAPTER 3:
Hardware and Software Setup

SDRs and commercially available software are used for practical application purposes. NI Ettus X310 SDRs are used for research flexibility and MIMO capabilities, which address the synchronization issues described in Chapter 2. GNU Radio is used because it is a commonly available open source SDR software with the ability to make custom functionality.

3.1 Hardware: Software Defined Radio and Antennas

The core hardware components in transmitting the signal are the SDRs and antennas.

3.1.1 NI Ettus X310 Software Defined Radio

NI makes SDRs with configurable hardware packages. The motherboards are built in. A Global Positioning System disciplined oscillator (GPSDO) can be added and the daughterboards are replaceable [11]. Digital signal processing (DSP) techniques are used instead of GPSDO to sync signals in this research.

The daughterboards include the hardware to transmit and receive the signal for a specific frequency spectrum. Since this research is designed for the HF range, the LFTX/RX (DC-30MHz) and Basic TX/RX (1-250MHz) daughterboards are the appropriate options. Both of these daughterboard types have dedicated transmit (TX) and receive (RX) components, as compared to the Twin daughterboards, which is a single transceiver [11]. The Basic TX/RX daughterboards are chosen to allow testing and troubleshooting flexibility via VHF and UHF bands.

X310 with overlaid labels is shown in Figure 3.1. The motherboard (blue labeling) is logically divided into two sides, each of which has a TX and RX section. These TX and RX sections are where the daughterboards (yellow labeling) are installed. Each daughterboard has connectors (red circular labeling) that are wired to the front end (bottom of picture not labeled) where the antennas or transmission lines connect. The benefit of the X310 over the X200 series is the resident capability to conduct 2x2 MIMO operations without

needing to connect multiple SDRs together with a special MIMO cable and synchronization hardware [11].

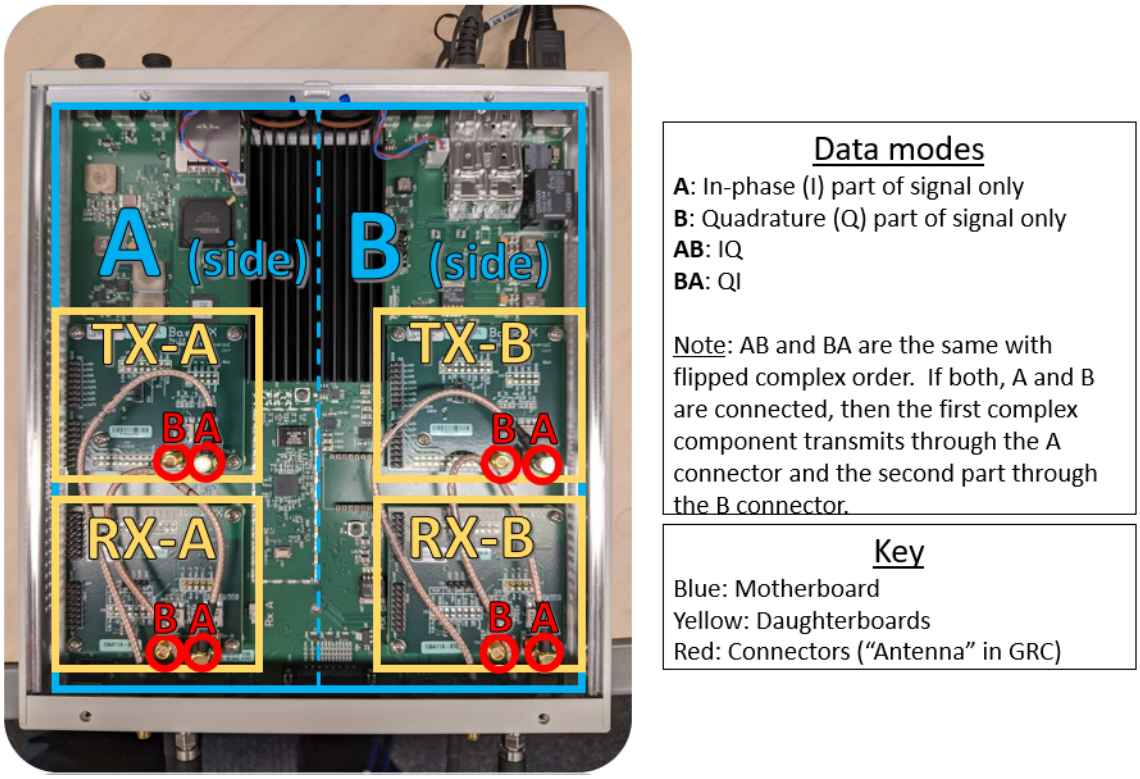

Figure 3.1. NI Ettus X310 SDR with two Basic TX and two Basic RX daughterboards (left) and data modes (Adapted from [11]) (right).

3.1.2 Antennas

The ideal length dipole for a 20 MHz antenna is resonant at 7.13 m with each element at 3.57 m, according to

$$\lambda = c/f, \tag{3.1}$$

where λ is the wavelength, c is the speed of light in the propagation medium, and f is the frequency [1].

The antennas used in lab tests and troubleshooting include 60.2 cm for VHF (Figure 3.2, top) [12] and 19.8 cm for UHF (Figure 3.2, bottom) [13]. Due to facilities-access restrictions imposed in response to the Coronavirus (COVID-19) pandemic, 7 m antennas are not tested.

The testing antennas are shorter than resonance for 20MHz, but the SNR is large enough in the lab environment (see section 3.2.3) to still produce successful results.

Figure 3.2. Antennas used for testing: 60.2 cm (top), 19.8 cm (bottom).

3.2 Hardware Configurations

Various stages of hardware setups are used. Only the setups used for presented results are described.

Four main configurations are used in this research: single SDR, SDR-to-SDR via cables (baseband only), SDR-to-SDR (MIMO setup) and SDR-to-SDR via antennas.

3.2.1 Baseband Configurations

Two configurations are used to up-convert and transmit the baseband signal: single SDR and SDR-to-SDR via cables.

The first is with a single SDR, which can be configured to either test the receive signal with a vector signal generator (VSG), as shown in Figure 3.3, or test the transmit signal with a spectrum analyzer (not shown).

Figure 3.3. Single SDR configuration with VSG to test TX baseband signal with RX flowgraph. Not shown: replace VSG with a spectrum analyzer to test TX flowgraph and view signal over the air.

The second configuration used for testing the baseband CEM signal transmitted on a carrier between two SDRs is shown in Figure 3.4. The SDRs are connected to a dual 10-gigabit Ethernet network interface card (NIC), as seen in Figure 3.5, and this configuration is tested successfully on one flowgraph. The SDRs are placed on different subnets to prevent direct communication at the NIC and ensure data is sent through the RF circuit.

Figure 3.4. SDR-to-SDR baseband configuration.

Figure 3.5. Dual NIC to connect two SDRs to one host computer.

3.2.2 Software Defined Radio to Software Defined Radio via Cables

The desired setup for this work is a 2x2 MIMO configuration, which requires using an additional transmit and receive connector pair (see Figure 3.6, left). Additionally, the OFDM-MIMO flowchart included DSP that requires both transmit signals to be combined, which also mimics how the signals of multiple antennas are coupled at the receiver. A combiner is added to merge the transmit signals, then a splitter is added to receive the combined signal at both receive connectors (see Figure 3.6, right). The combiner and splitter are made up of three 16.7-ohm resistors each. There are no diodes for current control [14]. The Basic TX/RX daughterboards do not have tunable or programmable gain controls built in. Gain blocks can be added outside of the universal software radio peripheral (USRP) blocks in flowgraphs or attenuators can be added to one of the cables in order to simulate multipath effects related to spherical spreading power loss [11].

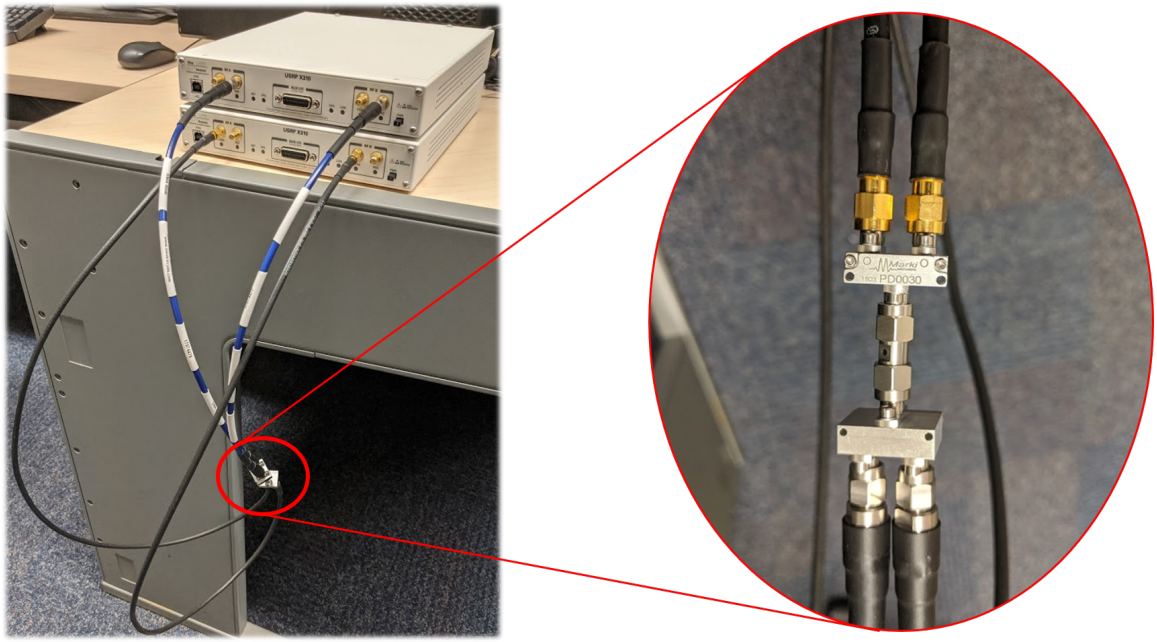

Figure 3.6. SDR-to-SDR via cables in MIMO-OFDM configuration (left) with emphasis on combiner and splitter (right).

3.2.3 Software Defined Radio to Software Defined Radio via Antennas

A carrier frequency of 20 MHz is still used, but the antennas are too short to meet resonance, affecting the received power. Since the lab environment is considerably small, the amplitude

loss from spherical spreading is minimal and ionosphere conditions could not be tested. To test in a multipath environment, the antennas are arranged in an endfire alignment and a barrier is placed between the SDR antennas to inhibit a line of sight (LOS) link. Both of these physical setups should provide a rich enough diversity of signals at the receiver.

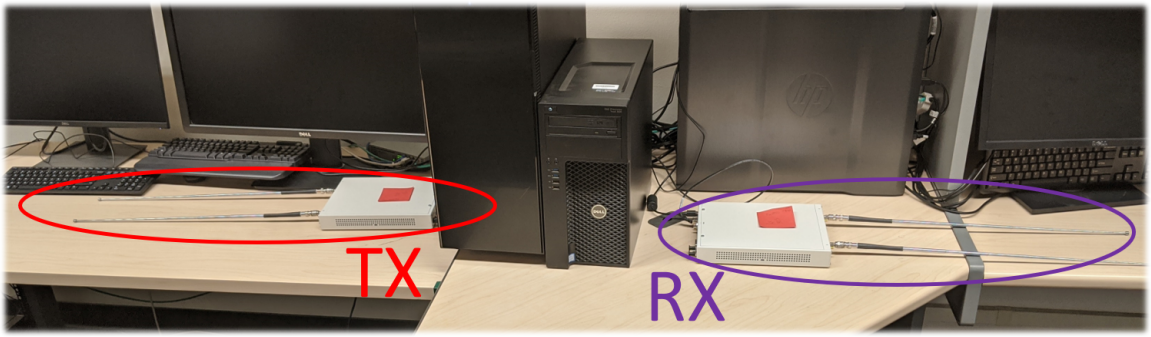

Figure 3.7. SDR-to-SDR configuration via antennas.

3.3 GNU Radio Companion

GNU Radio is a commonly used open source SDR software that uses Python and C to generate the desired functionality, which is converted into hardware description language (HDL) and written to the field-programmable gate array (FPGA) within the SDR. GRC is the flowgraph interface of GNU Radio [15].

3.3.1 Flowgraphs and Subsidiary Components

An example flowgraph is shown in Figure 3.8. GRC flowgraphs process the data in threaded functions, referred to as blocks. Sink and source nodes (colored connectors) transfer output of one block to the input of the next connected block and must be the same data type (same color). Data flow is controlled by input and output buffers and the computer operating system; the input, output, and manipulation of samples are controlled with various functions within each block. USRP blocks are used to interface with the X310 SDRs.

Important note: the subdev spec and antennas fields are different in the USRP blocks for Basic TX/RX and LFTX/RX daughterboard from that of Twin daughterboards. This

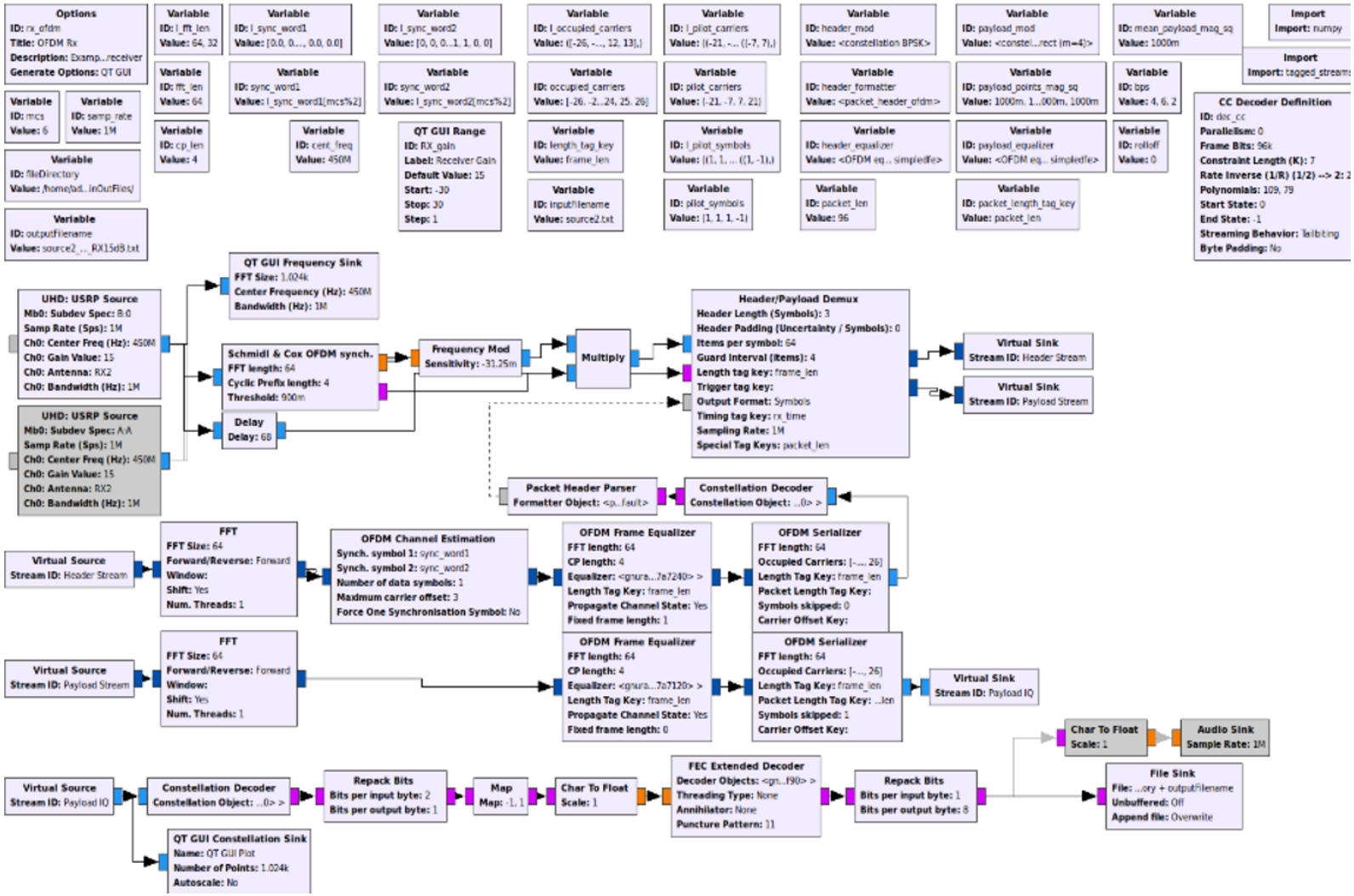

Figure 3.8. Example OFDM receive flowgraph with USRP blocks that interface with the X310. Source: [7].

research work uses Basic TX/RX daughterboards, which have a format per [11] and are depicted in Figure 3.1:

* Motherboards = [number of motherboards (blue); there is only one per X310] (i.e., 1)
* Subdev spec = [motherboard side(blue or yellow letter)]:[data mode] (i.e., B:AB)
* Antennas = [(red) connectors used] (i.e., A)

THIS PAGE INTENTIONALLY LEFT BLANK

CHAPTER 4:
N-Dimensional Constant Energy Modulation

CEM was developed as an extension of M-ary hyper phase shift keying (MHPSK) with improved spectral efficiency in non-linear channels. The concept of CEM focuses on using a multi-dimensional constellation that constrains the energy of all symbol vectors to a constant energy, while maximizing the minimum squared Euclidean distance between each symbol vector. Then symbol vectors are assigned Gray coded bit sequences. Transmitting multiple dimensions is solved by combining every two symbol vector components into complex subsymbols, which are transmitted via separate subcarriers. In other words, each signal vector may be thought of having phase constellations at each of the subcarriers utilized for the entire signal vector. Monte Carlo simulations showed BER performance improved as CEM dimensions increased and overall system performance was better with CEM in non-linear channels than equivalent existing modulation techniques [6].

4.1 Clarifying Terminology

Figure 4.1 is an example of 5D-128 CEM, which represents seven bits in five dimensions. Within the figure are the relationships between symbol vectors (S), subcarrier symbols (subsymbols), symbol components (s_n)/signal vector coordinate values (C_n), and dimensions.

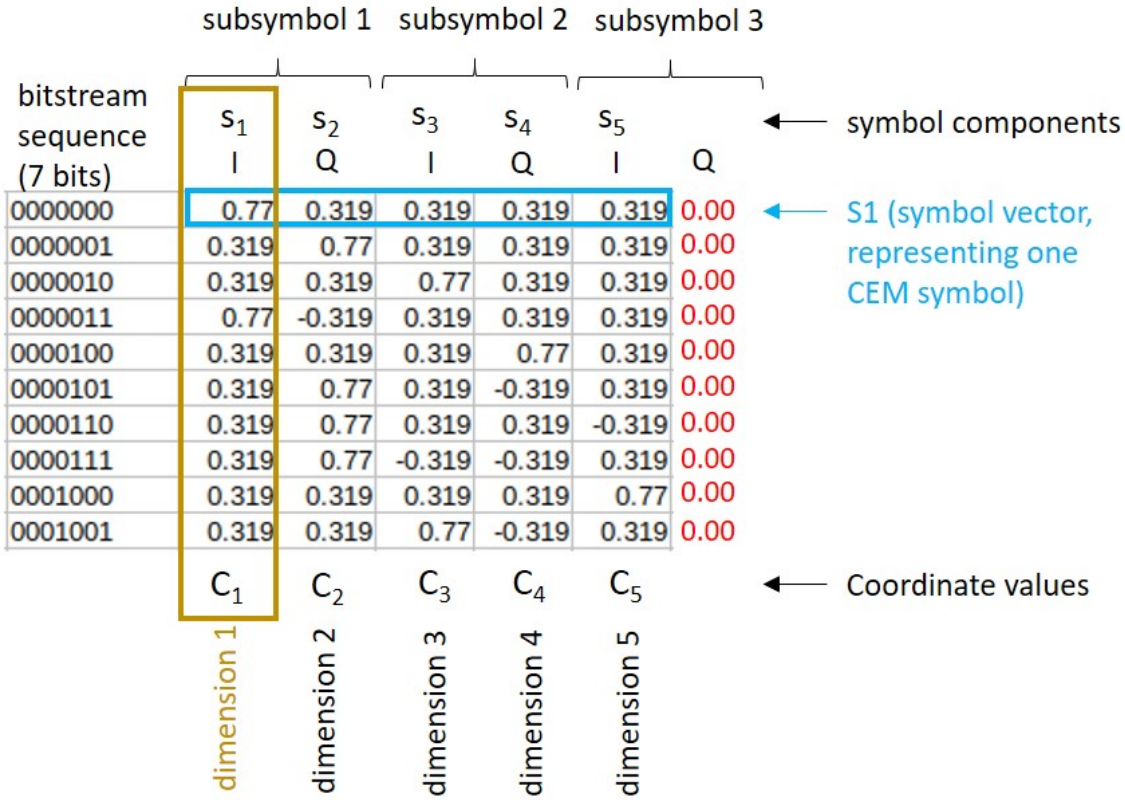

Figure 4.1. shows the first ten bit sequences, subsymbols, symbol vectors, and symbol components/coordinate values of the 5D-128 (7 bit) CEM symbols; the red zero values are added to pad the empty Q value in the last subsymbol for odd dimension constellations.

CEM symbols are represented by symbol vectors that are comprised of one symbol component per dimension. The values of the symbol components are signal vector coordinate values. Subsymbols ($s_{\text{odd}} + \text{j}s_{\text{even}}$) are complex-valued symbol component pairs that are transmitted over different subcarriers. If there is an odd number of dimensions, a value of zero is used for the quadrature component of the last subsymbol; this subsymbol is referred to as a padded subsymbol.

Constellations can be represented in three different ways with subcarrier implementation for CEM. The first form is a *multi-dimensional constellation*, which is made up of a complete signal vector. The second form is a *subsymbol phase constellation*, which is the phase

constellation of one subsymbol. The third form is a *combined subsymbol constellation*, which is the aggregate of all the subsymbol phase constellations as seen on a spectrum analyzer IQ map. All three forms are explained in this chapter. The multi-dimensional constellation will be referred to as a "constellation" as this form is the actual representation of the modulation. Subsymbol phase constellations and combined subsymbol constellations will be fully spelled out for clarity as these forms are unique to use of subcarriers for signal transmission.

4.2 Modulation Development

Each constellation was designed considering the number of bits, dimensions, energy constraint, and largest minimum squared Euclidean distance between symbol vectors [6].

4.2.1 Energy Constraint

The normalized constraint equation for N-dimensional signal constellations is

$$\sum_{j=1}^{n} r_j {C_j}^2 = 1, \tag{4.1}$$

where $n \leq N$, j=1, 2, 3, ..., n, and r_j is the number of times the j^{th} non-zero coordinate value, C_j, appears. Given that the maximum number of symbols per N-dimension is $2^N \times N!$, the maximum number of generated equal energy symbols, G, is

$$G = \frac{2^{n+m} N!}{r_1! r_2! r_3! ... r_n!}. \tag{4.2}$$

In practice, the number of transmitted signals is equal to or less than the maximum number of generated symbols. See Table 4.1 for dimensions 1-8. When the number of symbols desired is larger than $2^N \times N!$, the (N+1)-dimensional modulation needs to be used.

Table 4.1. Maximum number of generated and transmitted symbols for N-dimensional constant energy modulation. Source: [6].

N	Maximum Number of Generated Equal Energy Symbols (G)	Maximum Number of Transmitted Bits	Maximum Number of Transmitted Equal Energy Symbols (H)
1	2	1	2
2	8	3	8
3	48	5	32
4	384	8	256
5	3840	11	2048
6	46080	15	32768
7	645120	19	524288
8	10321920	23	8388608

BER is worse when symbols are closer. The largest minimum squared Euclidean distance, d^2_{min}, between constellation vectors is used to maximize the space between constellation points and provide the lowest BER. To achieve this, r_j and C_j are iterated in Equation (4.1). Then, the minimum squared Euclidean distance, d^2_{min}, for each case is calculated using Equations (4.3) to (4.7), where $\left|C_1\right| < \left|C_2\right| < \left|C_3\right| < ... < \left|C_n\right|$:

$$X = 2\left|C_1\right|^2, \tag{4.3}$$

$$Y = \left(2\left|C_1\right|\right)^2, \tag{4.4}$$

$$\begin{aligned} Z = \{2\left(\left|C_2\right| - \left|C_1\right|\right)^2, \;& 2\left(\left|C_3\right| - \left|C_1\right|\right)^2, \; 2\left(\left|C_4\right| - \left|C_1\right|\right)^2, \; ..., \; 2\left(\left|C_{n-1}\right| - \left|C_1\right|\right)^2, \\ & 2\left(\left|C_3\right| - \left|C_2\right|\right)^2, \; 2\left(\left|C_4\right| - \left|C_2\right|\right)^2, \; ..., \; 2\left(\left|C_n\right| - \left|C_2\right|\right)^2, \\ & 2\left(\left|C_4\right| - \left|C_3\right|\right)^2, \; ..., \; 2\left(\left|C_n\right| - \left|C_3\right|\right)^2, \\ & ..., \; 2\left(\left|C_n\right| - \left|C_{n-1}\right|\right)^2\}. \end{aligned} \tag{4.5}$$

The constellation is determined by using the largest d^2_{min} values. Equation 4.6 is derived

from Equations 4.3 to 4.5 and is used when one C_j has a value of zero:

$$d^2_{min} = min\left\{X, Y, Z\right\}, \text{excluding } Z = 2\left(\left|C_n\right| - \left|C_1\right|\right)^2. \tag{4.6}$$

Equation 4.7 is derived from Equations 4.4 and 4.5 and is used when all C_j have non-zero values:

$$d^2_{min} = min\left\{Y, Z\right\}, \text{excluding } Z = 2\left(\left|C_n\right| - \left|C_1\right|\right)^2. \tag{4.7}$$

4.2.2 Bit and Symbol Mapping

The algorithm proposed in [6] is visually depicted in Figure 4.2. Once the constellation is designed, the bit sequences are Gray coded and then sequentially mapped to symbol vectors based on increasing Euclidean distance from the reference vector. The reference vector is the symbol vector of the selected reference symbol used to design the constellation.

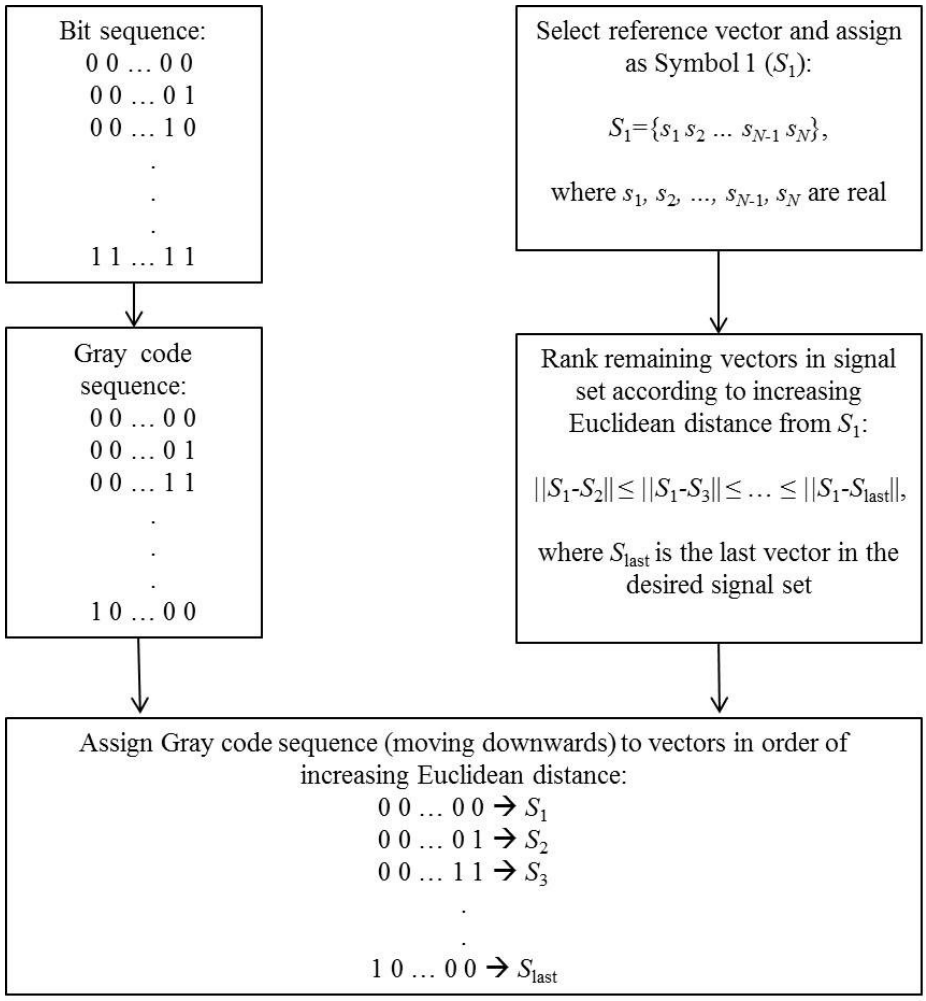

Figure 4.2. Flowchart of algorithm for CEM constellation design. Source: [6].

4.3 Baseband Modulation and Demodulation

The modulation and demodulation of CEM follow a similar method as OFDM where multiple subcarriers are filled with different subsymbols, which are transformed from/to the time domain with the fast Fourier transform (FFT)/inverse FFT (IFFT).

4.3.1 Modulation

The modulation process is shown in Figure 4.3 and the equivalent process in GRC is shown in Figure 4.4. The bit stream is read based on the number of bits per symbol, then mapped

to the corresponding symbols. The symbols are further mapped to the signal vectors. The symbol vector coordinate values are paired into complex subsymbols, which are then transformed to the time domain using the IFFT. The number of subcarriers used are the number of dimensions divided by two, then rounded up to the next largest integer (i.e., ceiling function). If there is an odd number of dimensions, then the remaining unassigned quadrature value in the last subsymbol is assigned a value of zero.

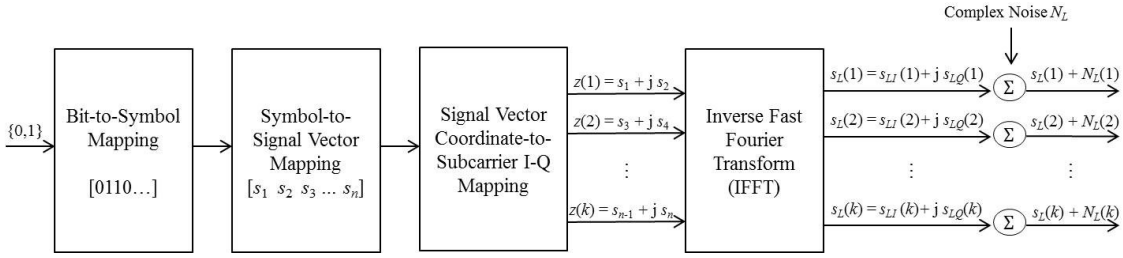

Figure 4.3. Block diagram of CEM modulator. Source: [6].

The GRC implementation of Figure 4.3 is Figure 4.4. The repack block sends the next number of bits based on the modulation bit size to the modulation block, which outputs subsymbols based on the number of subcarriers needed to transmit the desired amount of dimensions. The subsymbols are assigned to different subcarriers and converted to the time domain with the (reverse) FFT block.

The CEM modulation block is a custom out-of-the-tree block created in this work.

4.3.2 Demodulation

The CEM demodulation process is the reverse of the modulation process. The demodulation process is shown in Figure 4.5 and the equivalent process within GRC is shown in Figure 4.6. The received signal is the set of modulated subcarrier signals plus noise. The FFT is conducted on the subcarriers to transform the time signals into subsymbols. The noisy subsymbols are mapped into a noisy symbol vector. The minimum squared Euclidean distance detector acts as a matched filter using Euclidean distances to determine which symbol the noisy symbol vector most closely matches. The determined symbol is then mapped into corresponding bits.

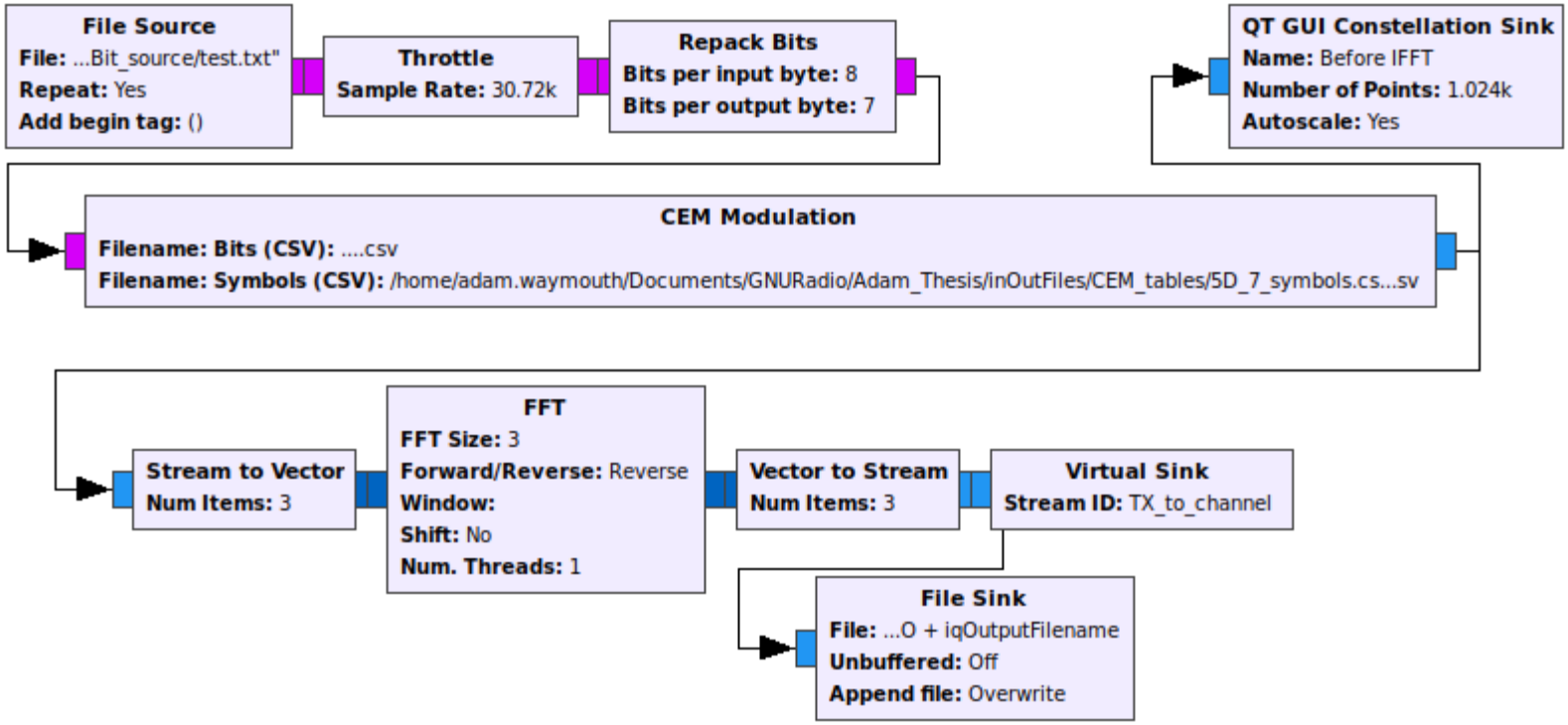

Figure 4.4. CEM modulation in GRC.

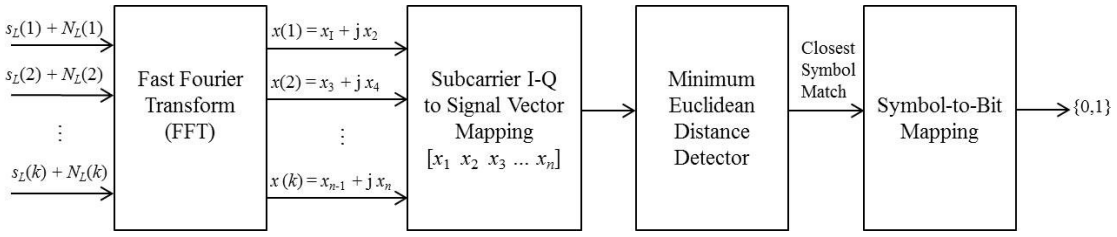

Figure 4.5. Block diagram of CEM demodulator. Source: [6].

The GRC implementation of Figure 4.5 is Figure 4.6. The FFT block converts the noisy subsymbols from the time domain into the frequency domain, which are scaled to retain the proper energy. The CEM demodulation block inputs the subsymbols, determines which constellation symbol vector is closest using the shortest Euclidean distance, and produces the associated bits. The bits are repacked into full bytes.

The CEM demodulation block is a custom out-of-the-tree block created in this work.

4.4 Baseband Comparisons

Various CEM constellations are analyzed. The 4D-16 CEM constellation and its BER are compared to QPSK and 16-QAM constellation and BER. CEM constellations will be referred to by the associated ND-M notation (i.e, 4D-16 vice 4D-16 CEM), where N is the selected number of dimensions, k is the selected number of bits, and $M = 2^k$ is the available number of symbols.

4.4.1 Constant Energy Modulation Constellations

Baseband versions of the combined subsymbol constellations are used for analysis because the amount of subcarriers used in transmission changes the representation of the combined subsymbol constellation and is not consistent for analysis. All combined subsymbol constellations are shown in baseband before being assigned subcarriers.

ND-N^2 Constellations

When $k = N$, the CEM combined subsymbol constellation is considered balanced and classified as a ND-N^2 constellation. Balanced constellations are also referred to as *filled*

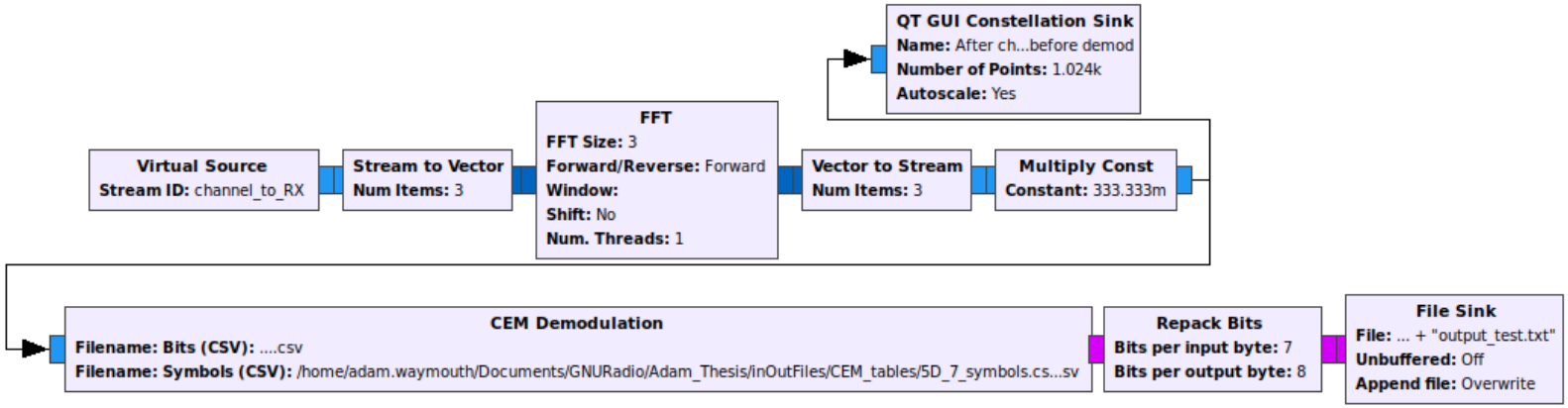

Figure 4.6. CEM demodulation in GRC.

constellations. The 4D-16 and 6D-64 constellations are shown in Figures 4.7 and 4.8, respectively; both are even ND-N^2 constellations where k is even and equals N. Even ND-N^2 constellations resemble QPSK in shape, but with different scaled energy; odd ND-N^2 constellations do not (i.e, Figure 4.9). The scaled energy is reduced more as dimensions are increased, but are assigned to more subcarriers when transmitted. This inverse relationship of reduced energy and increased subcarriers is due to symbol energy constraints as defined in Equation 4.1. For example, QPSK at unit energy has in-phase and quadrature components of ±0.707 for one subcarrier, 4D-16 has in-phase and quadrature components of ±0.5 for two subcarriers, and 6D-64 CEM has in-phase and quadrature components of ±0.4082 for three subcarriers.

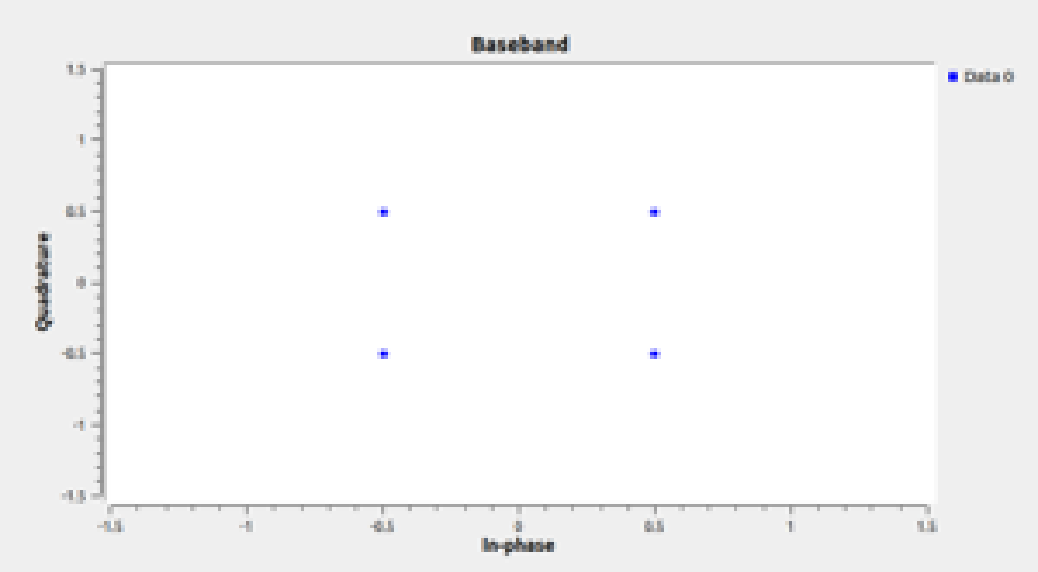

Figure 4.7. 4D-16 combined subsymbol constellation.

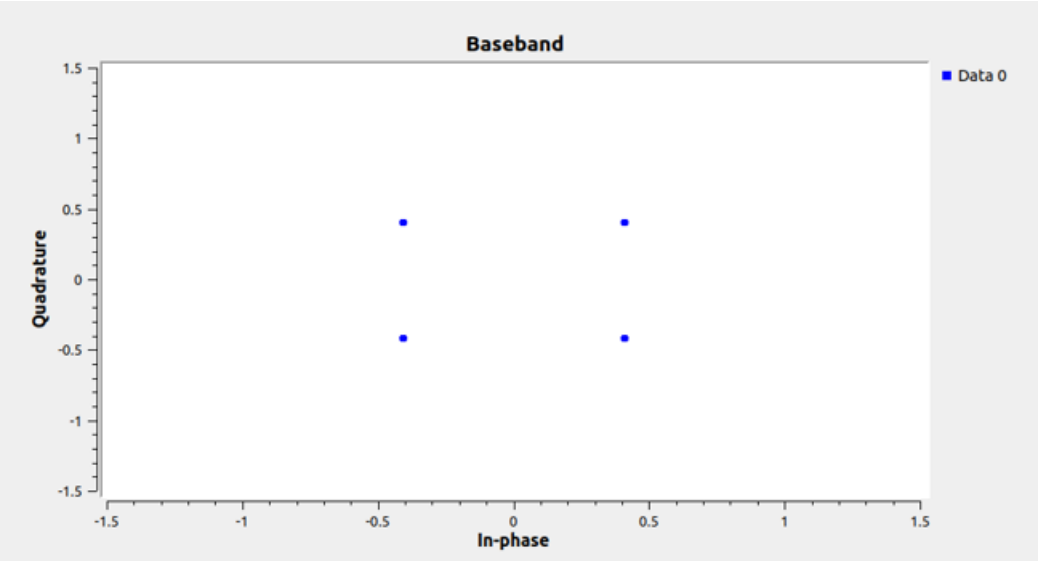

Figure 4.8. 6D-64 combined subsymbol constellation.

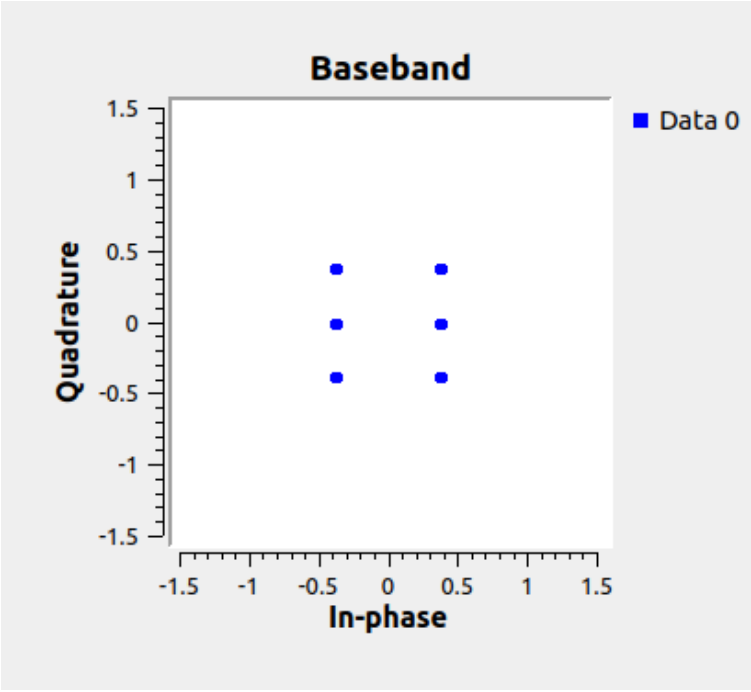

Figure 4.9. 7D-128 combined subsymbol constellation.

Overfilled Constellations

When $k \neq N$, the CEM combined subsymbol constellation is not balanced and can be defined as either an *overfilled* constellation ($k > N$ case) or an *underfilled* constellation ($k < N$ case). Underfilled constellations can be made, but are not considered in this work. Figures 4.10, 4.11, 4.12, 4.13, and 4.14 contain overfilled constellations, which reveals a pattern where the corners of the combined subsymbol constellations are not present when $k \geq N + 2$. QAM constellations have corner points that require higher energy values to produce. Non-linear amplifiers are common in RF applications. Non-linear amplifiers used with QAM constellations may limit the power, which pulls the outside points closer to the next nearest points, causing inter-symbol interference (ISI). This can explain why CEM performs better when using non-linear amplifiers than comparable QAMs.

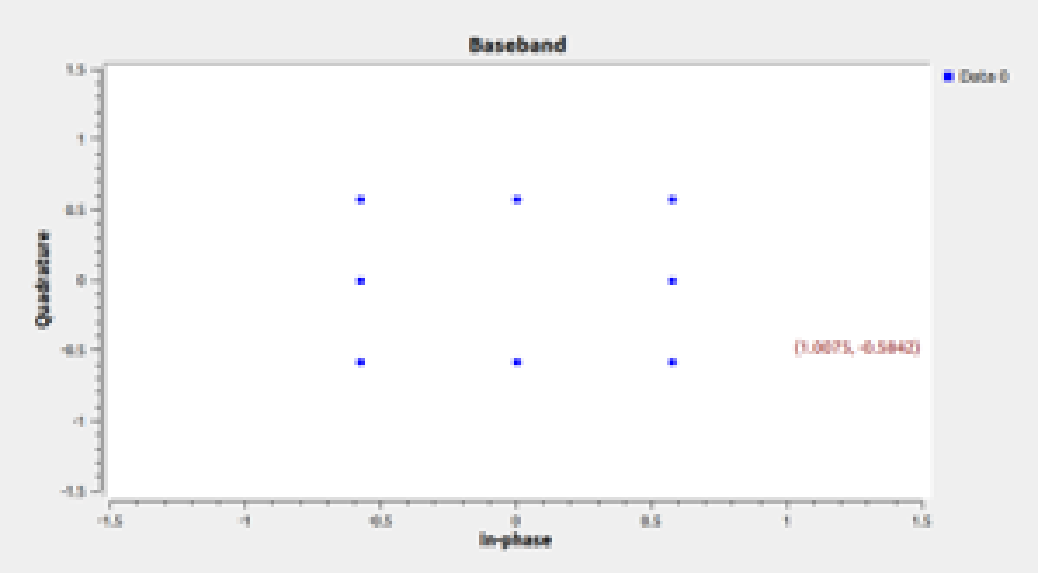

Figure 4.10. 4D-32 combined subsymbol constellation.

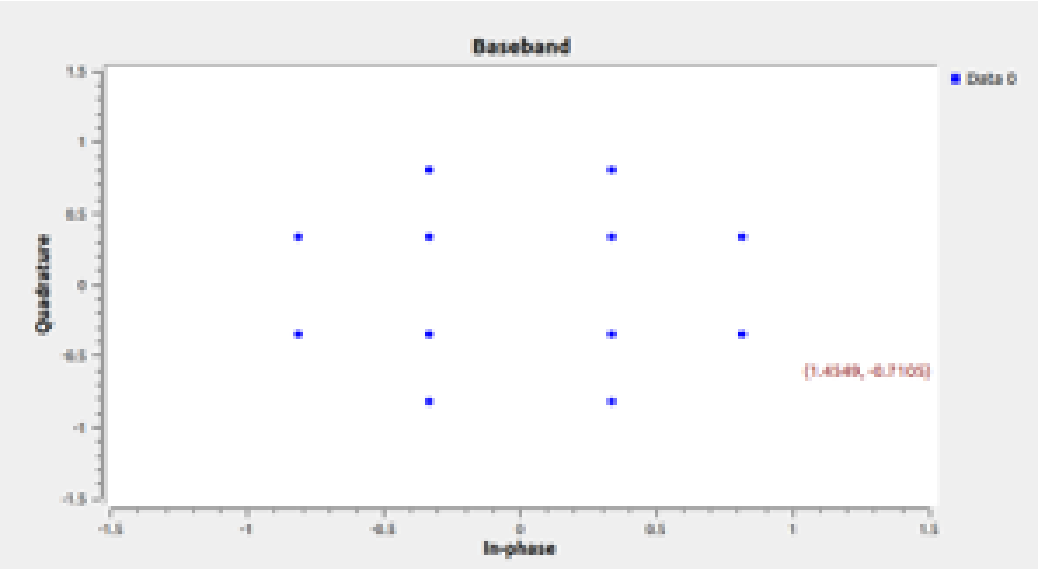

Figure 4.11. 4D-64 combined subsymbol constellation.

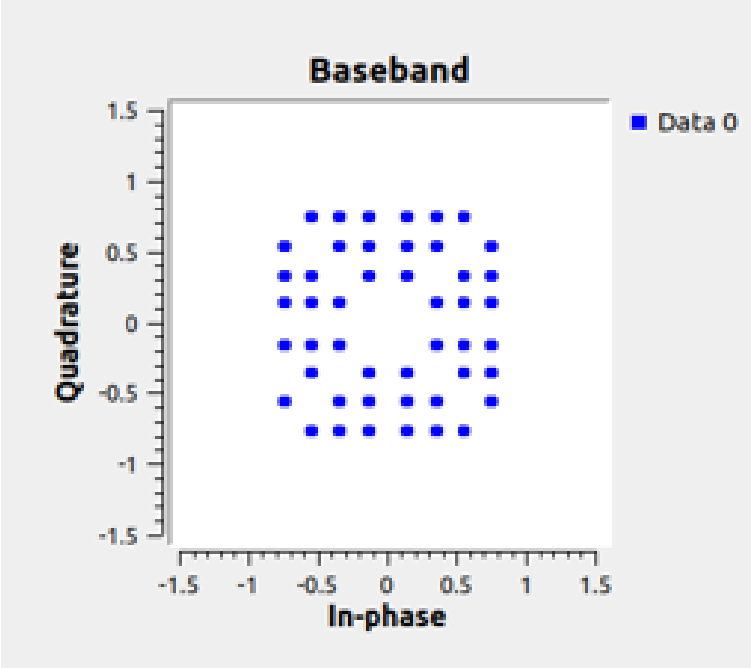

Figure 4.12. 4D-256 combined subsymbol constellation.

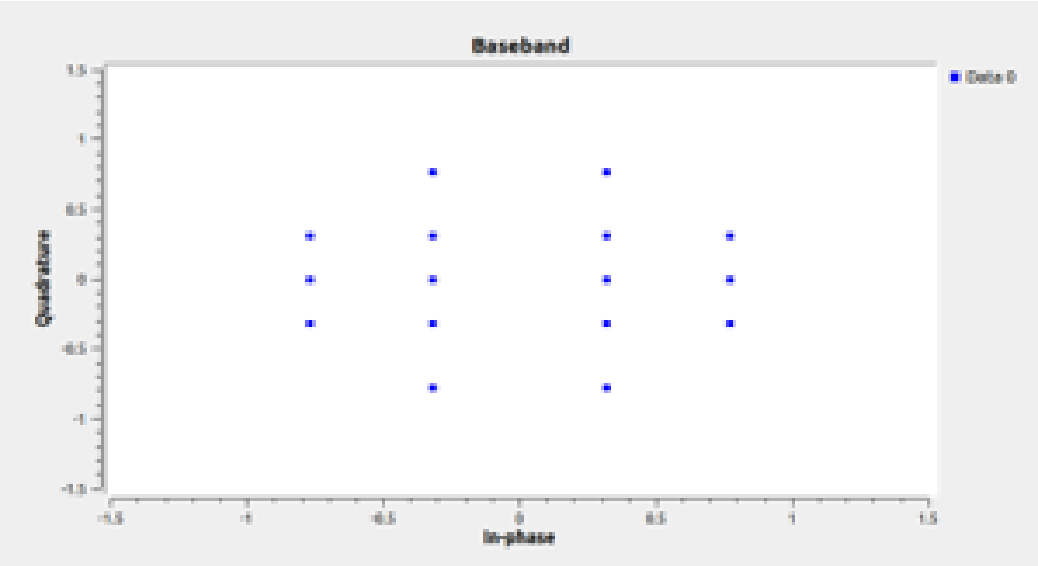

Figure 4.13. 5D-128 combined subsymbol constellation.

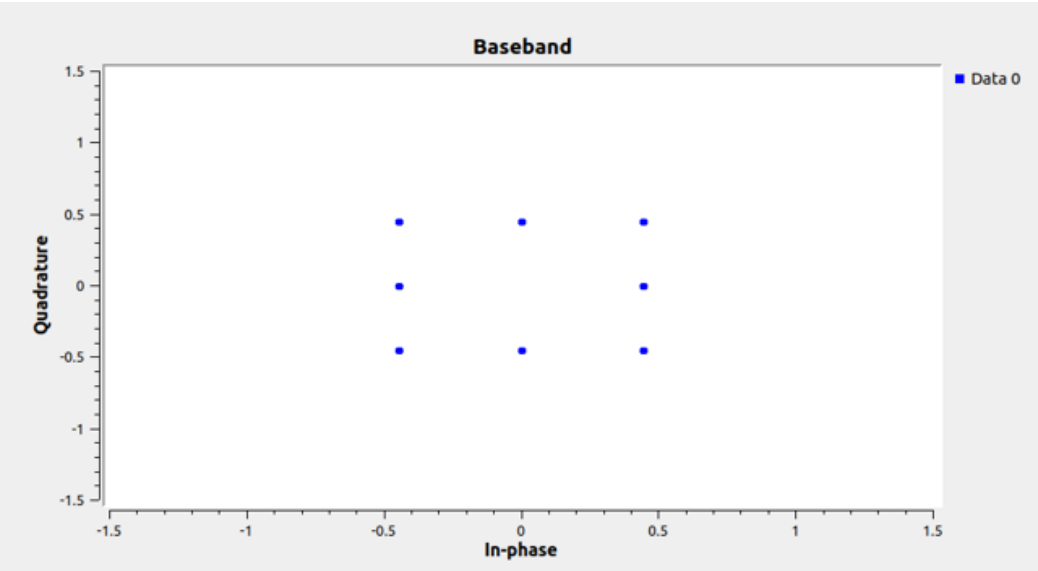

Figure 4.14. 6D-128 combined subsymbol constellation.

Zero-Valued Subsymbols

Baseband CEM symbol vectors do not produce zero-valued subsymbols, but some odd ND-M constellations have a zero value in the highest dimension. This work assignes a

zero value for the quadrature component of the last odd ND-M subsymbol, creating a padded subsymbol. When the highest dimension of an odd ND-M has a zero, the padded subsymbol becomes a zero-value subsymbol. The zero-valued subsymbol is represented in the baseband constellation (i.e., Figure 4.15). During transmission, the SDR does not transmit on the antenna assigned the zero-valued subsymbol. The flowgraphs created in this research are able to identify the zero-valued subsymbol at the receiver and able to correctly demodulate symbol vectors to bit sequences.

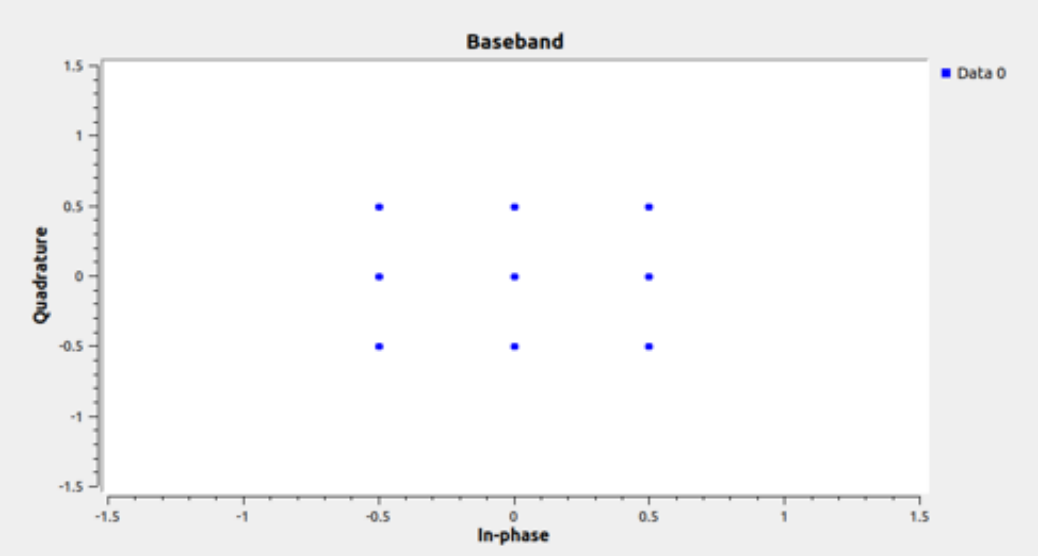

Figure 4.15. 5D-64 combined subsymbol constellation.

4.4.2 4D-16 Constant Energy Modulation Comparisons

Figure 4.16 compares QPSK, 4D-16, and 16-QAM constellations and shows how the modulation represents the associated symbol(s) for an example bit sequence.

Figure 4.17 compares the BER of QPSK, 4D-16, 4D-32, 4D-64, and 16-QAM.

Constellation Comparison

The 4D-16 constellation is compared to QPSK because the subsymbol phase constellations and combined subsymbol constellations have the same shape and similar bit sequence representation as a QPSK constellation. The two subcarriers used to transmit one 4D-16

symbol are represented in the top center of Figure 4.16 and the entire 4D-16 symbol is represented in the bottom center as viewed on a spectrum analyzer. Two time instances of QPSK on one subcarrier or one time instance of two QPSK symbols on two subcarriers has the same representation as one 4D-16 symbol.

The 4D-16 constellation is compared to 16-QAM because both transmit the same number of bits per modulated symbol. 4D-16 is shown to be more spectrally efficient than 16-QAM.

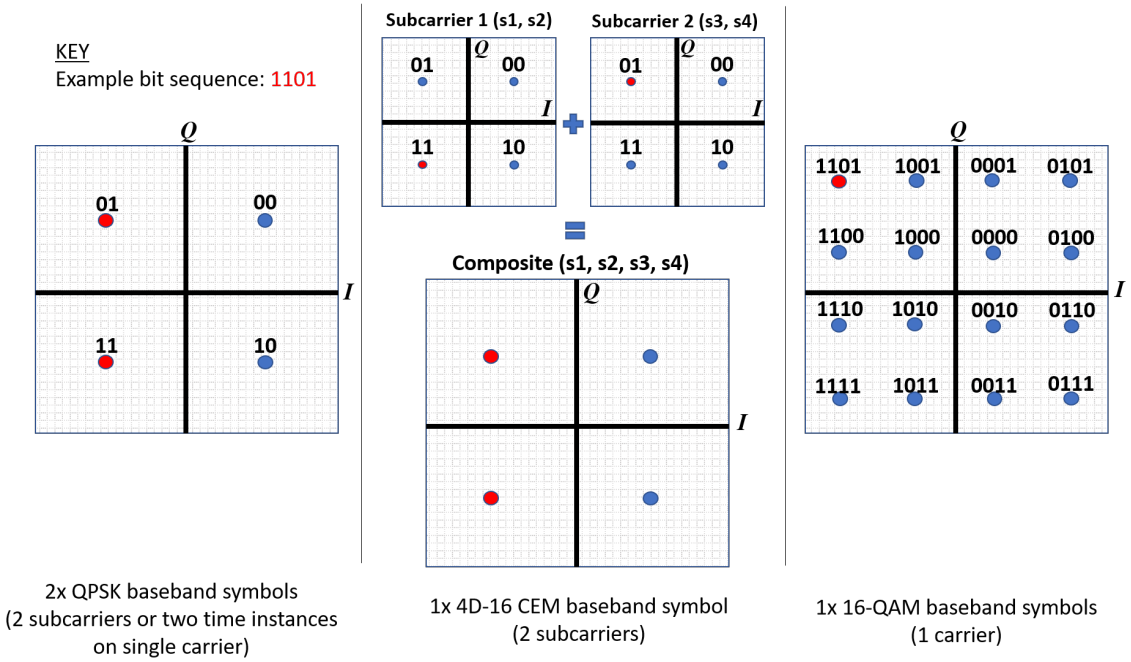

Figure 4.16. Comparison of modulation constellations: QPSK (left), 4D-16 CEM (center), and 16-QAM (right).

Bit Error Rate Comparison

BERs for CEM are reported via bounded closed-form theoretical approximations in [6] and compared to typical modulations.

The 4D-16 BER is comparable to the QPSK BER in Figure 4.17. The BER for CEM worsens as the number of bits is increased for the same number of dimensions. 4D-32 and 4D-64 transmit more bits per symbol than 16-QAM single carrier and have a lower BER.

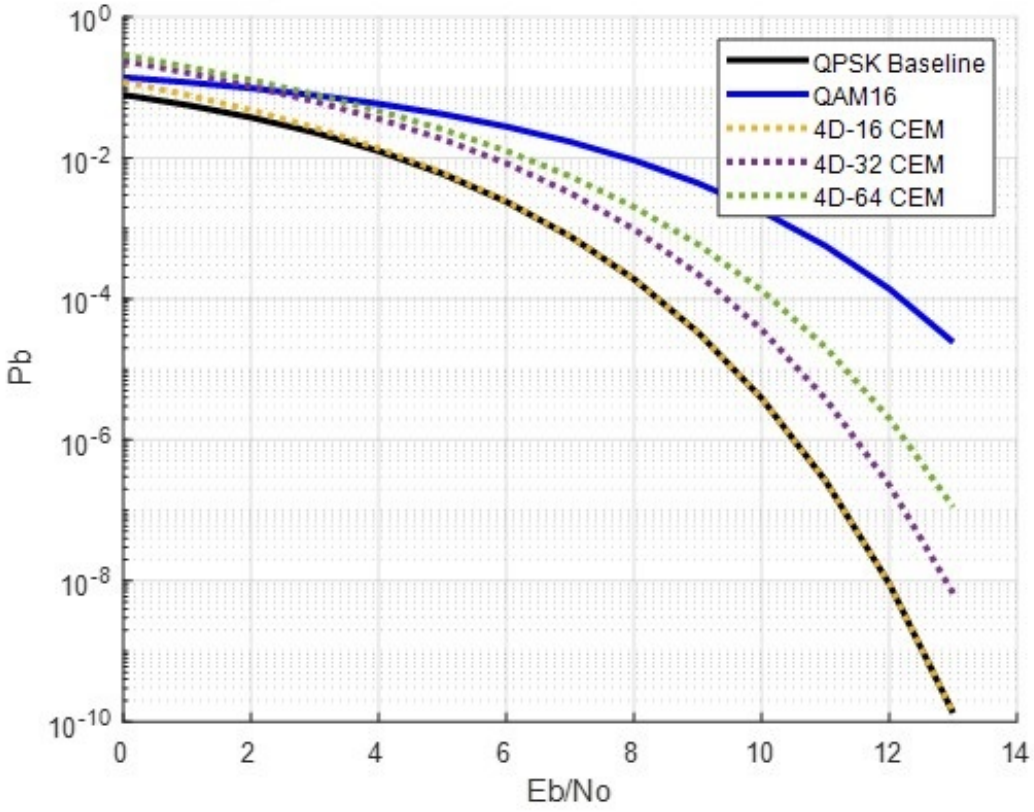

Figure 4.17. Comparison of QPSK, various 4D CEM, and 16-QAM BERs.

CHAPTER 5:
Communication Architecture

The SDR-to-SDR setups with cables and antennas are used with the MIMO-OFDM flowcharts. The transmit and receive flowgraphs are created together for GNU-only tests, then are separated for tests between SDRs. The transmit flowgraph needs to be started prior to the receive flowgraph so that the automatic gain controller in the receive flowgraph uses the correct gain coefficient.

5.1 Transmit Flowgraph

The entire transmit flowgraph is shown in Figure 5.1. The data set is modulated into subsymbols, encoded in accordance with the Alamouti code, placed on ODFM subcarriers, and then transmitted with an SDR.

5.1.1 Transmit: Modulation

The modulation portion of the transmit flowgraph is shown in Figure 5.2. The modulation is the same as explained in section 4.3.1. Forward error correction (FEC) is added to mitigate the effects of a deep fade.

5.1.2 Transmit: Multiple-Input Multiple-Output

The MIMO portion of the transmit flowgraph is shown in Figure 5.3. The Alamouti Encoder takes the modulated subsymbols and produces STBC symbols. A training sequence is added for channel estimation to mitigate slow or fast fading and improve synchronizing the signal at the receiver.

5.1.3 Transmit: Orthogonal Frequency Division Multiplexing

The OFDM portion of the transmit flowgraph is shown in Figure 5.4. OFDM Carrier Allocator assigns the STBC symbols to the subcarriers, thus making OFDM symbols. FFT and Vector to Stream transform the OFDM symbols to the time domain for transmission.

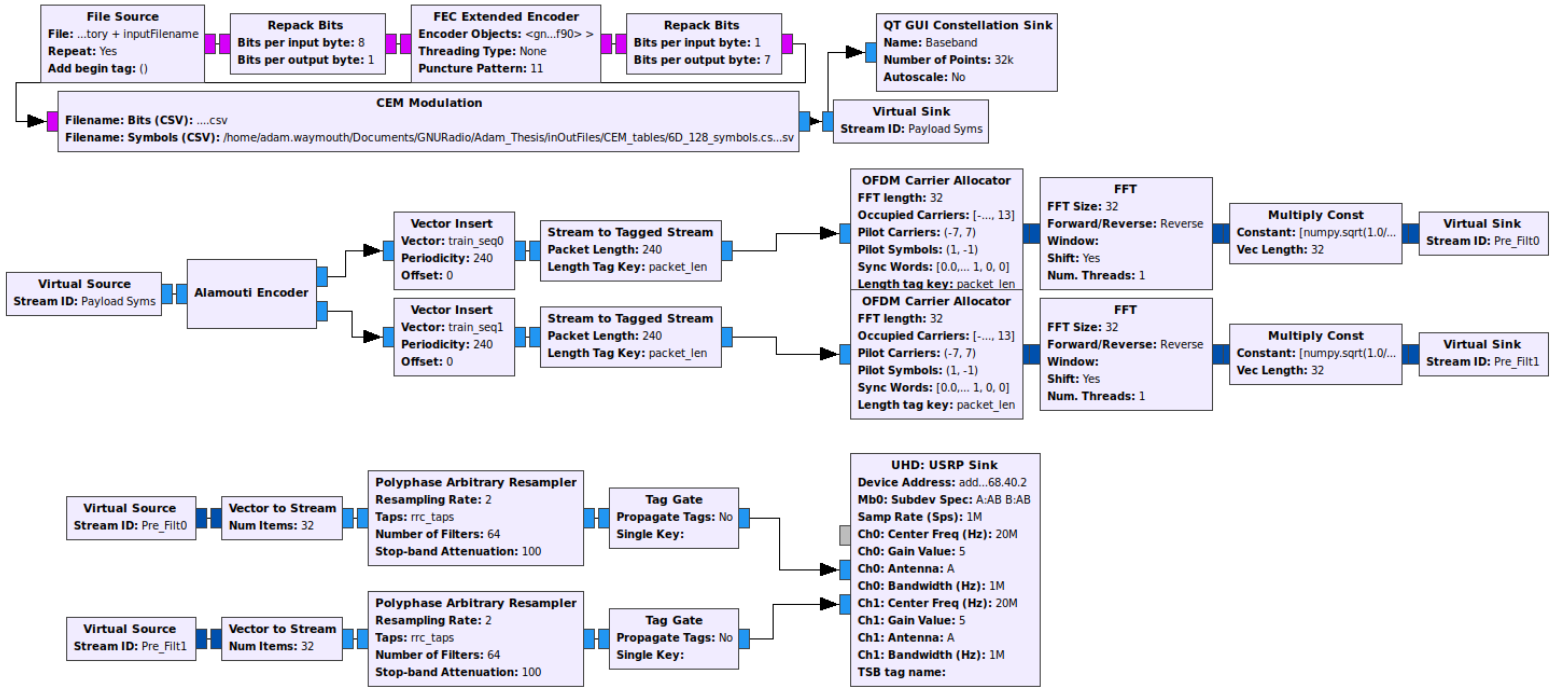

Figure 5.1. MIMO-OFDM CEM transmit flowgraph.

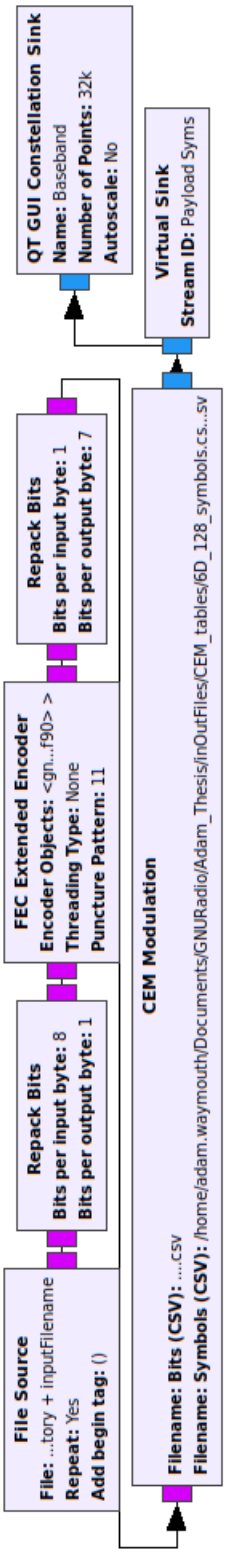

Figure 5.2. MIMO-OFDM CEM transmit flowgraph - modulation.

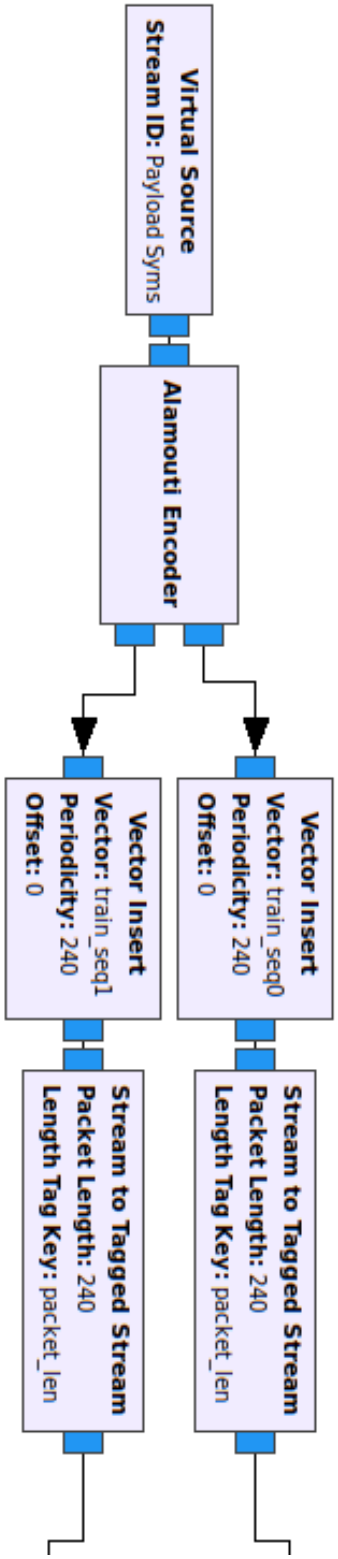

Figure 5.3. MIMO-OFDM CEM transmit flowgraph -MIMO.

Figure 5.4. MIMO-OFDM CEM transmit flowgraph - OFDM.

5.1.4 Transmit: Transmission

The transmission portion of the transmit flowgraph is shown in Figure 5.5. The Polyphase Arbitrary Resampler conducts a root rasied cosine pulse shaping to the signal and passes the signal to the USRP Sink for transmission via the SDR.

5.2 Receive Flowgraph

The entire receive flowgraph is shown in Figure 5.6. The receive flowgraph reverses the process of the transmit flowgraph in order to extract the transmitted data.

5.2.1 Receive: Signal Synchronization

The receive and synchronization portion of the receive flowgraph is shown in Figure 5.7. The USRP Source imports the signal to the flowgraph from the SDR. AGC2 (automatic gain controller) amplifies the signal. For the AGC2 to determine the right amplification value, the transmit flowgraph needs to be running prior to starting the receive flowgraph. The Polyphase Clock Sync synchronizes the signal. Adding the resultant magnitudes of both FFT Filters produces an auto correlation that the MIMO Frame Synchronizer uses to find the training sequence. The signal is synchronized prior to entering the OFDM section.

5.2.2 Receive: Orthogonal Frequency Division Multiplexing

The OFDM portion of the receive flowgraph is shown in Figure 5.8. The signal is vectored and transformed to the frequency domain. The OFDM Channel Estimation uses sync words to determine the channel effects and passes to the OFDM Frame Equalizer to correct. The OFDM Serializer does the reverse of the OFDM Allocator from the transmit flowgraph by outputting the symbols to a stream.

5.2.3 Receive: Multiple-Input Multiple-Output

The MIMO portion of the receive flowgraph is shown in Figure 5.9. MISO (Alamouti) Single Tap Channel Estimator uses the training sequence to determine the channel estimation used by the MIMO (Alamouti) Single Tap Channel Equalizer to correct channel effects. Keep M in N block removes the training sequence from the stream.

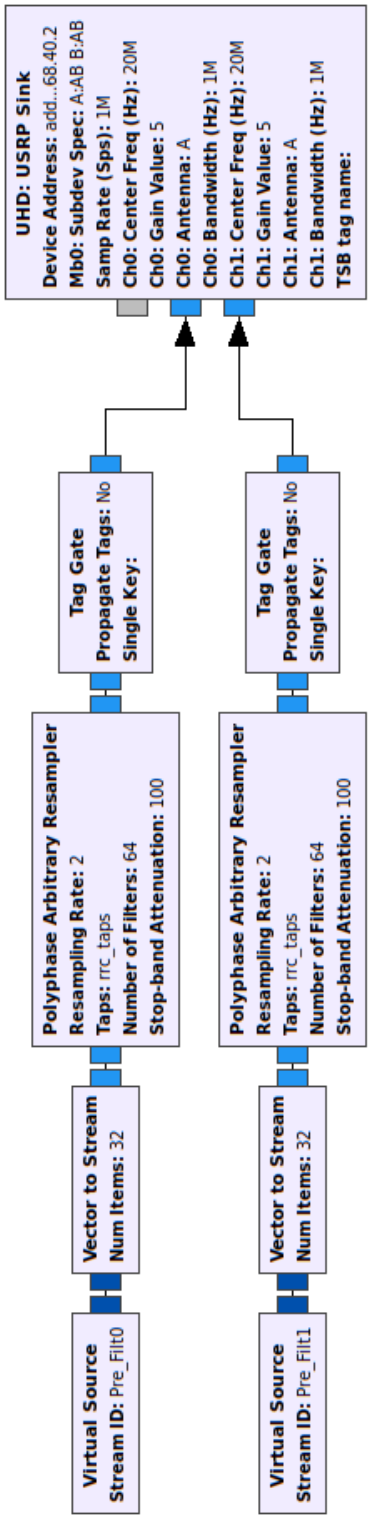

Figure 5.5. MIMO-OFDM CEM transmit flowgraph - transmission.

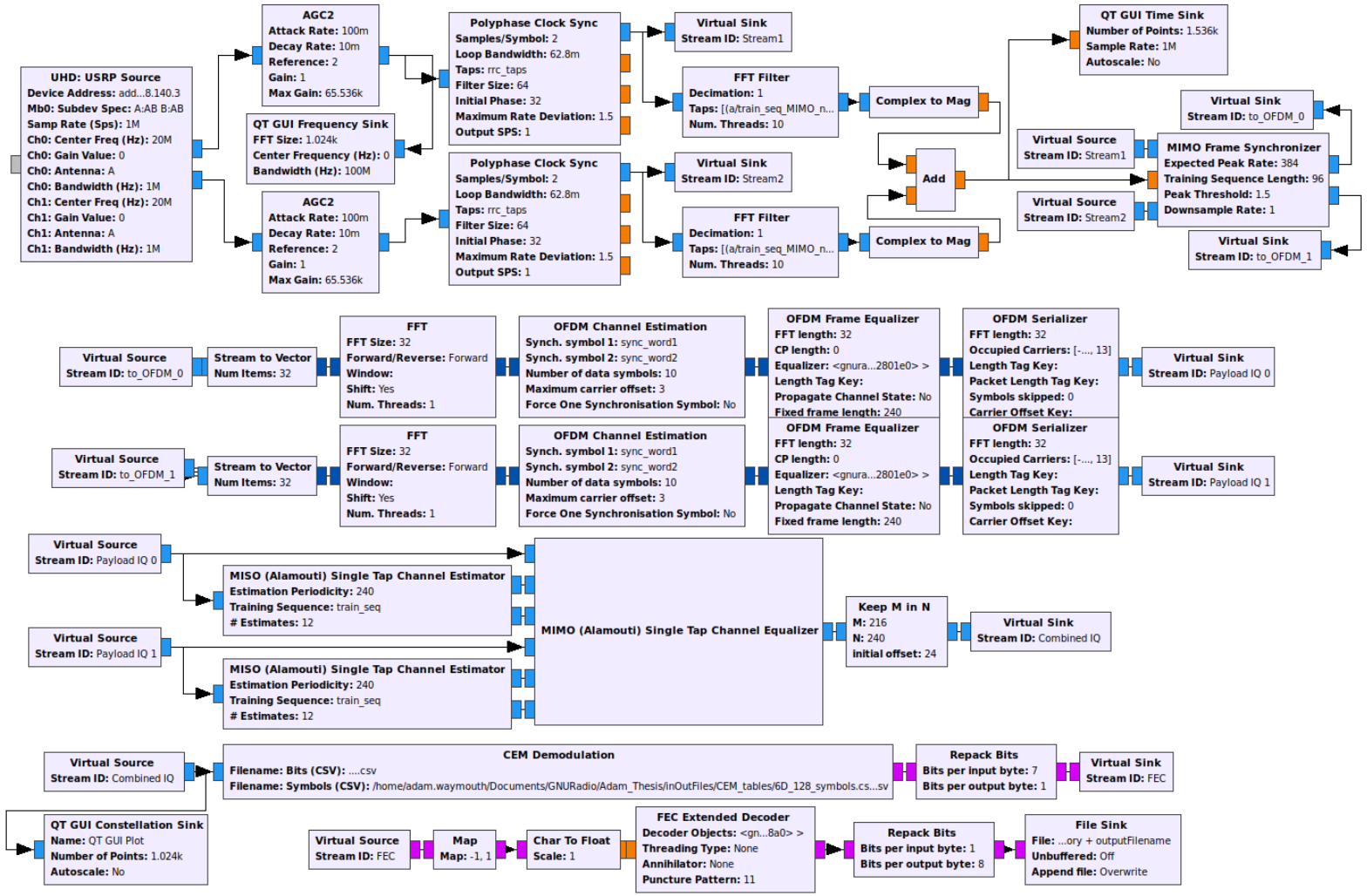

Figure 5.6. MIMO-OFDM CEM receive flowgraph.

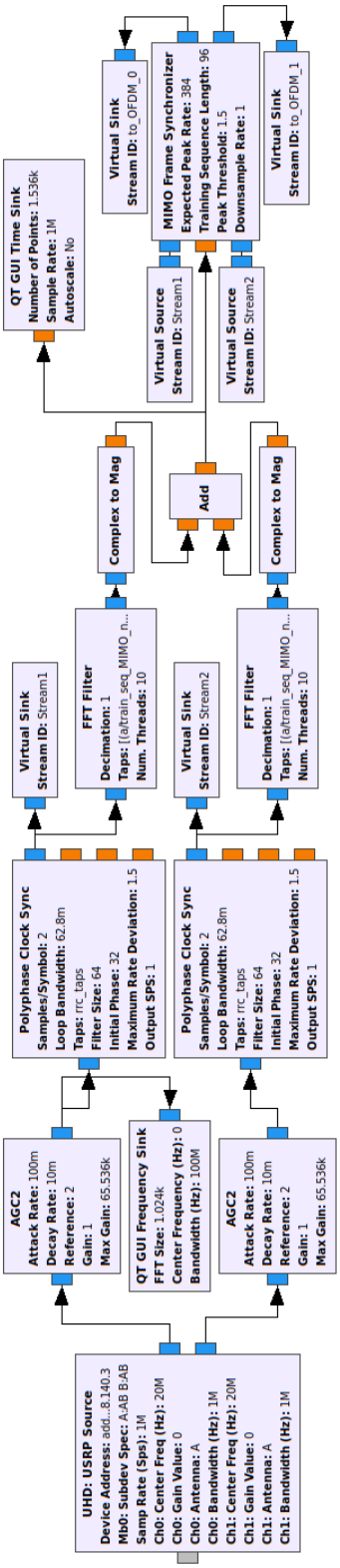

Figure 5.7. MIMO-OFDM CEM receive flowgraph - synchronization.

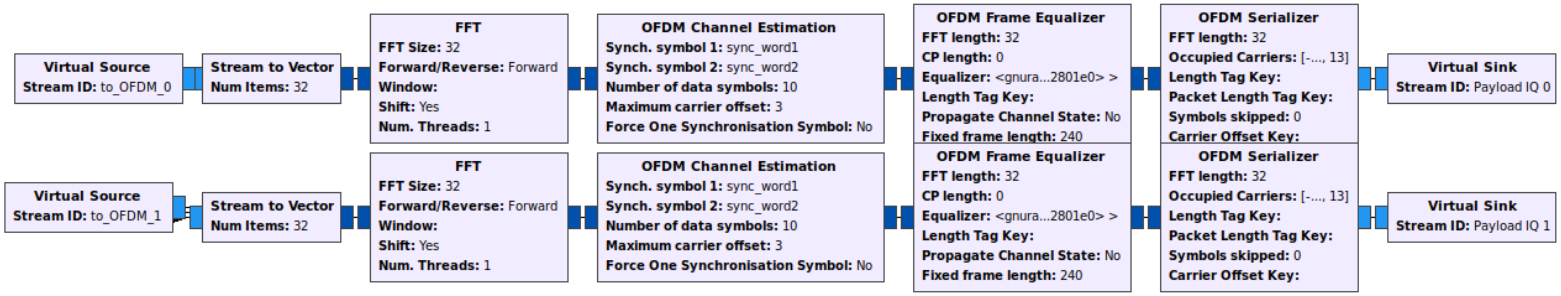

Figure 5.8. MIMO-OFDM CEM receive flowgraph - OFDM.

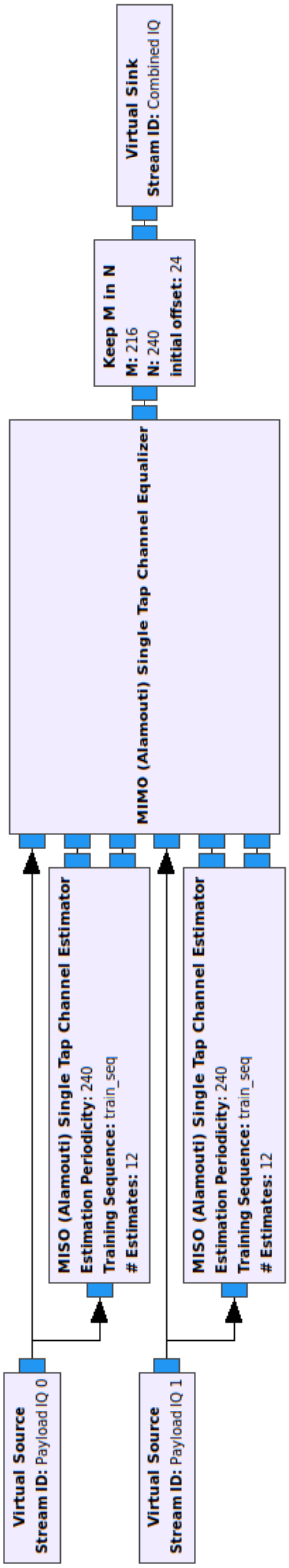

Figure 5.9. MIMO-OFDM CEM receive flowgraph -MIMO.

5.2.4 Receive: Demodulation

The demodulation portion of the receive flowgraph is shown in Figure 5.10. The demodulation works the same as explained in section 4.3.2. Map and FEC Extended Decoder blocks conduct the error correction adjustments to counter deep fading. The data is saved to the specified file.

5.3 Additional Considerations

The CEM MIMO-OFDM architecture can be enhanced with additional benefits.

5.3.1 Padded Subsymbols

Padding the quadrature component of a padded subcarrier with a zero value maintains constant energy, but is partially an inefficient use of the subsymbol. Two possible ways to use the empty quadrature component are to implement error detection and/or correction using *symbol component parity* similar to other checksum parity checks and to implement *subsymbol sharing*, where the last symbol component of a symbol vector share the subsymbol with the first symbol component of the next symbol vector. Applying a non-zero value to the quadrature component will violate the constant energy constraint that defines CEM, thus the coordinate values of all component symbols need to be scaled based on the energy of the quadrature component. Additionally, if the quadrature value of a padded subcarrier is the same energy of another component symbol component value, then it can look like an even ND-M constellation and introduce dimension uncertainty to an eavesdropper.

5.3.2 Physical Layer Security

Dimension uncertainty with padded subsymbols is introduced in section 5.3.1. Other potential physical layer security methods are introduced in this section.

Network layer encryption protects data with specialized hardware that can increase costs or with specialized software that can increase processing [16], [17]. Physical layer solutions protect the information on the waveform and can either supplement network layer encryption to protect more sensitive data, or can replace current encryption systems to reduce system costs and data processing for less sensitive data.

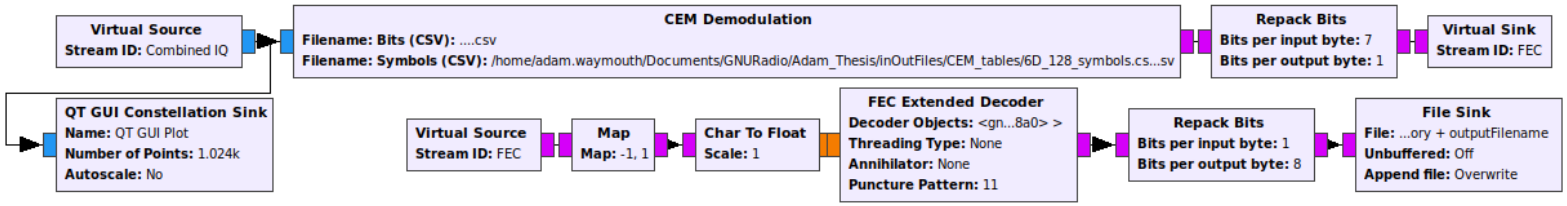

Figure 5.10. MIMO-OFDM CEM receive flowgraph - demodulation.

Previous researchers [4], [18] have theorized and simulated multiple methods to use STBCs for physical layer security. Our work does not directly study or implement either STBC physical layer security methods, but does setup the foundational RF circuit for follow-on research and testing. Additionally, to properly retrieve the correct symbols from the Alamouti code, the correct MIMO antenna configuration must be known. Changing the antenna configuration will not prevent against a replay attack, but can increase costs and time for an eavesdropper to demodulate the signal.

5.3.3 OFDM Frequency Agility With Narrowband Noise Mitigation

The foundational work for this research showed the ability to select which subcarriers contain symbols, and thus improve SNR by omitting subcarriers in a degraded channel [7]. A theoretical example using CEM is shown in Figure 5.11.

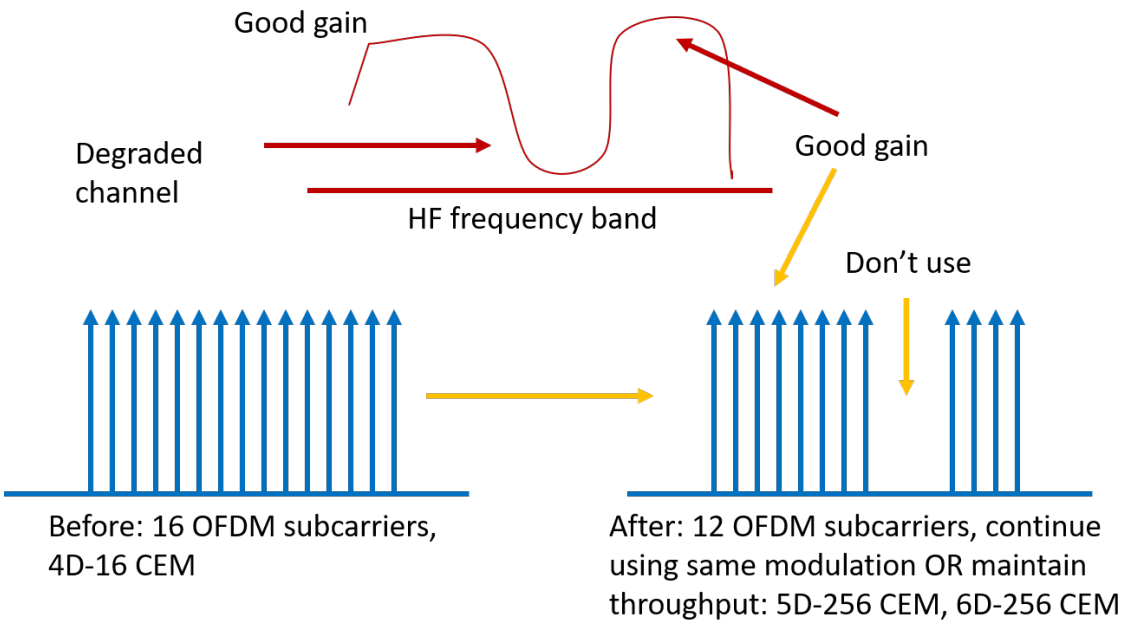

Figure 5.11. OFDM subcarriers removed to mitigate degraded channel. Adapted from [7].

Experimental results of [7] using GNU Radio Companion, one NI Ettus X310 SDR, and a Rhode & Schwarz signal generator proved that removing subcarriers and reassigning the

symbols to remaining subcarriers still allowed data to be transmitted and received effectively. A successful QPSK demodulation and constellation is demonstrated in Figure 5.12.

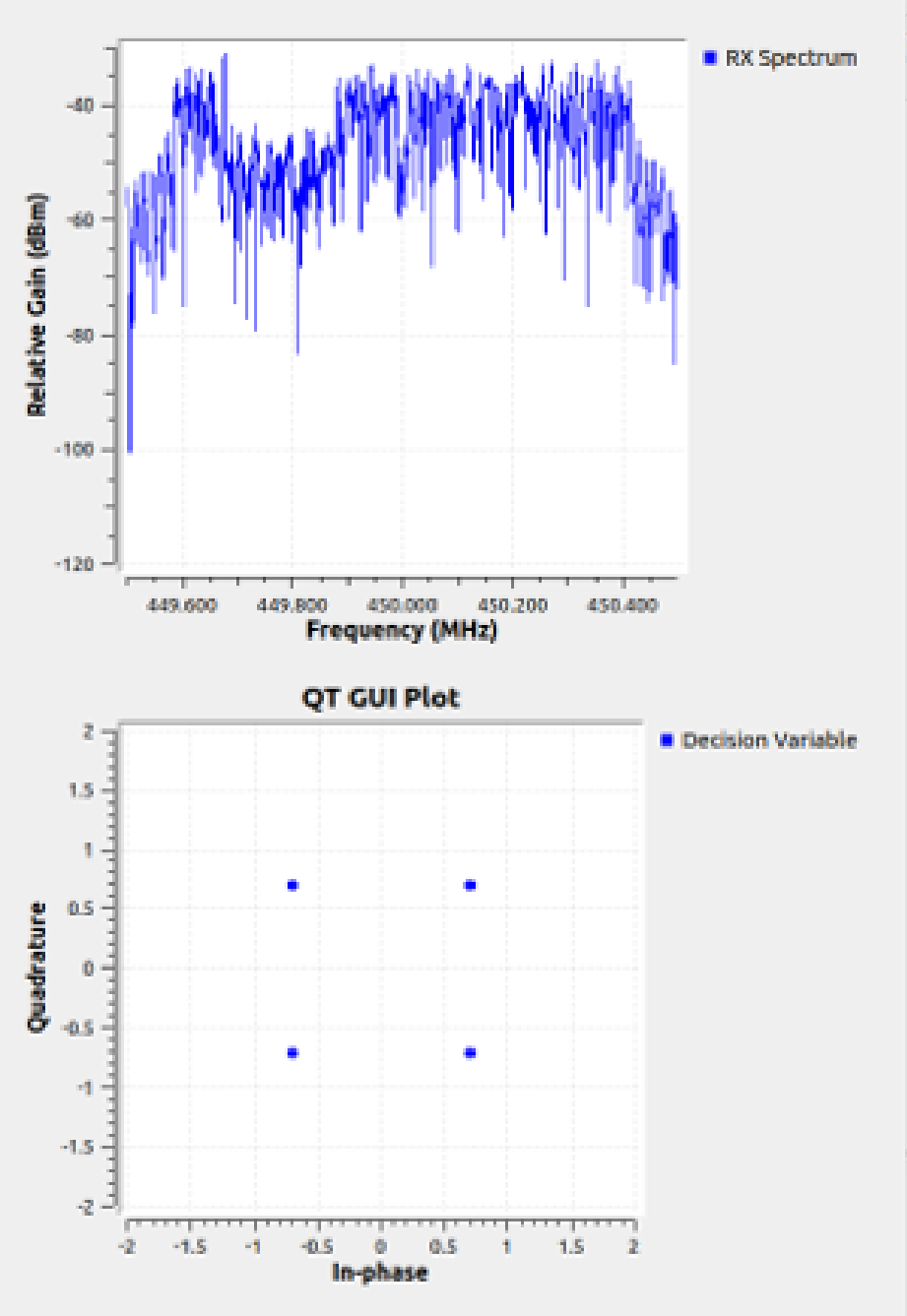

Figure 5.12. Successful demodulation of QPSK with partial OFDM subcarriers. Source: [7].

To maintain data throughput when removing subcarriers, the bits per symbol needs to be increased, which is accomplished by changing the modulation [7]. CEM provides the flexibility to change either the amount of bits per symbol or the number of dimensions to meet throughput requirements when removing OFDM subcarriers during narrowband noise mitigation.

Thus, the overall BER may improve when compared to using all subcarriers with the same narrowband noise. Atmospheric soundings, propagation modeling tools, and spectrum analyzers can be used to identify degraded channels [7]. Dynamically assigning subcarriers during military operations can provide frequency agility for electronic maneuver warfare and contribute to Command and Control of the battle space. Commercial shipboard use can benefit from improved BER. For both military and commercial scenarios, CEM can provide unique and flexible modulation solutions to maintaining desired data throughput when the number of OFDM subcarriers change.

CHAPTER 6:
Conclusions and Recommendations

Conclusions and recommendations for future work are included.

6.1 Conclusions

While the concept of MD-CEM was first introduced in [6], its initial implementation in terms of transmission and reception via cabled and over-the-air experiments is first demonstrated in this work. CEM constellations were presented, demonstrating constellation variations. 4D-16 CEM was compared to QPSK and 16-QAM. Analysis of CEM constellations explained why CEM had improved performance with non-linear amplifiers when compared to QAM. The CEM MIMO-OFDM architecture mitigated the affects of fading and allowed for inclusion of STBC physical layer security and frequency agility using dynamic OFDM subcarrier management. CEM was a flexible modulation class that could provide modulation agility in conjunction with OFDM subcarrier management to maintain desired data throughput.

6.2 Recommendations

Recommendations for future work include the following ideas. It is suggested to improve processing, increase usable dimensions in CEM GNU blocks, and analyze performance metrics with tactical units. It is advised to develop a scheme for subsymbol sharing to improve throughput of odd dimension variations and remove zero-valued subsymbols. We recommend to create a cognitive sensing adaption of MIMO-OFDM architecture by incorporating OFDM subcarrier agility/CEM modulation agility. We propose incorporating STBC physical layer security, OFDM subcarrier agility, and CEM modulation agility into a communications-embedded OTH radar. We suggest using CEM modulation agility to dynamically optimize data throughput versus Eb/No. It is advised to explore physical layer implications and applications in CEM. Finally, we recommend to create error correction methods using constant energy constraint or using the quadrature component of padded subcarriers.

THIS PAGE INTENTIONALLY LEFT BLANK

List of References

[1] C. A. Levis, J. T. Johnson, and F. L. Teixeira, *Radiowave Propagation: Physics and Applications*. Hoboken, NJ, USA: Wiley, 2010.

[2] E. Altmann. (2013, Dec 20). BFTN(e) Multi-Layer Spatial Multiplexer (MLSM) for RF Networking. *(SBIR) Navy - BFTN(e) Multi-Layer Spatial Multiplexer (MLSM) for RF Networking*. [Online]. Available: https://www.navysbir.com/n14_1/N141-079.htm

[3] PE 0204163N / Fleet Tactical Development. (2017, May). R-1 Line #204. in Exhibit R-2, RDT&E Budget Item Justification: FY 2018 Navy. Available: https://www.dacis.com/budget/budget_pdf/FY18/RDTE/N/0204163N_204.pdf

[4] M. Cribbs, R. Romero, and T. Ha, "Orthogonal stbc set building and physical layer security application," in *2020 IEEE 21st International Workshop on Signal Processing Advances in Wireless Communications (SPAWC)*, 2020, pp. 1–5.

[5] R. A. Romero, Y. E. Heng, and T. T. Ha, "N-dimensional m-ary constant energy modulation for nonlinear communications channels," in *2019 IEEE-APS Topical Conference on Antennas and Propagation in Wireless Communications (APWC)*, 2019, pp. 093–096.

[6] Y. Heng, "Multi-dimensional constant energy modulation," M.S. thesis, Dept. Electron. Eng., Naval Postgraduate School, Monterey, CA, 2013.

[7] A. J. Waymouth and R. Romero, "Improving Digital HF with OFDM," presented at MechAero 2019, San Fransisco, CA, Sep 2019.

[8] S. V. B. Rao, T. R. Rao, V. G. Reddy, D. R. Lakshmi, B. Veenadhari, R. S. Dabas, I. Ahmed, M. M. Gupta, and B. M. Reddy. (2002, Oct). HF radio signal fading and atmospheric radio noise measurements at low latitudes. *AGU Journals*. [Online]. Available: https://agupubs.onlinelibrary.wiley.com/doi/pdf/10.1029/2001RS002495

[9] T. T. Ha, *Theory and Design of Digital Communication Systems*. Cambridge, UK: Cambridge University Press, 2011.

[10] O. A. Ekwe, A. E. Abioye, M. O. Oluwe, and K. Okoro, "Effective fading reduction techniques in wireless communication system," in *IOSR Journals*. Figshare, 2014, pp. 093–096.

[11] Ettus Research. (2020, Aug 11). Daughterboard Properties. *USRP Hardware Driver and USRP Manual: Daughterboards*. [Online]. Available: https://files.ettus.com/manual/page_dboards.html

[12] Paskernack Enterprises. (2020, Aug 19). Antennas Technical Data Sheet: PE51TW1000. *Paskernack Enterprises*. [Online]. Available: https://www.pasternack.com/images/ProductPDF/PE51TW1000.pdf

[13] Paskernack Enterprises. (2020, Aug 19). PE51087 Rubber Duck Antenna2400-2500 &4900-5825 MHz, 2.5dBi. *Pasternack Enterprises*. [Online]. Available: https://www.pasternack.com/images/ProductPDF/PE51087.pdf

[14] Marki Microwave. (2019, May). PD-0030. [Online]. Available: https://www.markimicrowave.com/Assets/datasheets/PD-0030.pdf

[15] GNU Radio. (2020, May). Guided Tutorial GNU Radio in Python. *Guided Tutorial GNU Radio in Python - GNU Radio*. [Online]. Available: https://wiki.gnuradio.org/index.php/Guided_Tutorial_GNU_Radio_in_Python

[16] D. B. C. Writer. (2015, Jun). Tales from the Crypt: Hardware vs Software. *Infosecurity Magazine*. [Online]. Available: https://www.infosecurity-magazine.com/magazine-features/tales-crypt-hardware-software

[17] Ontrack. (2020, Aug 14). Hardware Encryption vs. Software Encryption: The Simple Guide. [Online]. Available: https://www.ontrack.com/en-us/blog/hardware-encryption-software-encryption

[18] E. A. Watson, "RF Exploitation of WIMAX," M.S. thesis, Dept. Electron. Eng., Naval Postgraduate School, Monterey, CA, 2011.

Initial Distribution List

1. Defense Technical Information Center
   Ft. Belvoir, Virginia

2. Dudley Knox Library
   Naval Postgraduate School
   Monterey, California